Progress in Particle and Nuclear Physics 129 (2023) 104007

Contents lists available at ScienceDirect

Progress in Particle and Nuclear Physics

journal homepage: www.elsevier.com/locate/ppnp

Review

# Equation of state for QCD from lattice simulations

Claudia Ratti

*Physics Department, University of Houston, Houston TX 77204, USA*

ARTICLE INFO

*Article history:*
Available online 23 November 2022

*Keywords:*
Quantum Chromodynamics
Quark-Gluon Plasma
Equation of State

ABSTRACT

I will review the state of the art of the equation of state for strongly interacting matter from first principles. I will discuss results at zero and finite chemical potential. For the latter, I will focus on Taylor expansion, analytical continuation from imaginary chemical potential, and a novel expansion scheme that was recently introduced, and that allowed a substantial extension of the coverage in baryonic chemical potential. I will also introduce a few lattice-based approaches, used to study the thermodynamics in the vicinity of the critical point.



**Contents**

1. Introduction ... 2
2. QCD thermodynamics from the lattice ... 2
3. QCD equation of state at $\mu_B = 0$ ... 3
   3.1. Integral method ... 4
   3.2. High temperature, ideal gas limit ... 5
   3.3. Results ... 7
4. Equation of state at finite chemical potential ... 8
   4.1. Fermionic sign problem ... 8
   4.2. Thermodynamics at finite chemical potential ... 9
   4.3. Taylor expansion ... 9
   4.4. Simulations at imaginary chemical potential ... 11
      4.4.1. Simulation setup ... 11
   4.5. Results ... 13
   4.6. Resumming Taylor expansions ... 14
   4.7. A novel expansion scheme ... 15
      4.7.1. Motivation ... 15
      4.7.2. Formalism ... 16
      4.7.3. Lattice determination of the expansion coefficients ... 17
      4.7.4. Thermodynamics at real chemical potential ... 18
   4.8. Other observables at finite chemical potential ... 20
5. Other approaches at high chemical potential ... 20
   5.1. Dyson–Schwinger equation ... 20
   5.2. Equation of state in the black hole engineering approach ... 20
   5.3. Lattice-based approach with a 3D-Ising model critical point ... 21
6. QCD at finite isospin chemical potential ... 22
7. Conclusions ... 25
   Acknowledgments ... 25

*E-mail address:* cratti@Central.UH.EDU.

https://doi.org/10.1016/j.ppnp.2022.104007
0146-6410/

Appendix ..... 25
References ..... 27

## 1. Introduction

Ultrarelativistic heavy-ion collisions currently taking place at the Relativistic Heavy-Ion Collider (RHIC) [1–4] and at the Large Hadron Collider (LHC) [5–7] systematically create the quark–gluon plasma in the laboratory. This phase of matter, a deconfined soup of quarks and gluons, permeated the Universe just a few microseconds after the Big Bang and it only exists in extreme conditions of temperature and density.

The fundamental theory of strong interactions, Quantum Chromodynamics, can only be solved numerically in the regime which is relevant for heavy-ion experiments. These simulations on a discretized lattice in space and Euclidean time are currently limited to vanishing and small values of the baryonic chemical potential, due to the fermionic sign problem. The theory predicts that the transition from hadrons to quarks and gluons is an analytical crossover [8], but it is expected to become first-order at high baryonic densities [9–12]. This would mean that there is a critical point on the QCD phase diagram [13]. The search for the elusive critical point is the focus of the RHIC experimental program. The STAR experiment has also developed a fixed target program to further extend their reach to larger densities [14]. The HADES experiment at the GSI (Darmstadt) [15] covers even larger densities with the potential of a beam energy scan as well. Since the conditions achieved in low energy heavy ion collisions [16] have an overlap with those achieved in neutron star mergers [17], information about the QCD critical point and phase diagram can also be obtained from observations of gravitational waves [18].

The equation of state of strongly interacting matter is therefore crucial for several fields of physics, from heavy-ion collisions to neutron stars and mergers. The reason why we do not know it over the whole phase diagram yet is that the fermionic sign problem prevents its direct calculation at finite density. In this manuscript, I will review the existing results in the literature for the equation of state at zero and finite baryonic chemical potential, focusing on the Taylor expansion, analytical continuation from imaginary chemical potential, and a new expansion scheme that was recently proposed in Ref. [19].

## 2. QCD thermodynamics from the lattice

The lattice discretization of a field theory is based on its path-integral representation: in the case of QCD, the partition function can be expressed as a Euclidean path integral over quark and gluon fields. The former are Dirac spinors $\bar{\psi}_f$, $\psi_f$, the latter are SU(3) vector fields $A_\mu$. The partition function depends on the temperature $T$, volume $V$, quark masses $m_f$ and chemical potentials $\mu_f$ for quarks of flavor $f$. The theory is considered in the Euclidian space–time, by replacing the real time $t$ with an imaginary one, $t \to -ix_4$, with real $x_4$. This is done so that we can apply powerful techniques developed in statistical mechanics to this problem. While in the continuum limit we have only one theory of strong interactions, the lattice discretization of the space–time defines the lattice field theory under study. Different discretizations give rise to different theories, which should all converge to QCD in the continuum limit. We will consider 4-dimensional hyper-cubic lattices $N_s^3 \times N_t$ with three spatial dimensions $N_s$ and a temporal dimension $N_t$. The temperature $T$ is the inverse of the size of the lattice in the temporal direction: $T = 1/(N_t * a)$, with $a$ the lattice spacing in physical units. The lattice points are called sites. The bonds connecting the nearest neighbor sites are called links. Quark fields are defined on the sites, gauge fields live on the links $U_\mu(x) = \exp(iaA_\mu(x))$. Starting from the continuum Euclidean QCD action, the simplest way of discretizing it is by replacing the derivatives by finite differences. This trivial action is however affected by severe discretization effects, which can be reduced by e.g. including further differences in the derivative than just the nearest neighbors.

Fermions on the lattice are complicated to treat. In addition to the physical mode, there are so-called "doublers", which arise because the derivative in the kinetic term of the Dirac action is first order. These unwanted modes survive as relevant degrees of freedom in the continuum limit, where they all converge to the same mass. However, at finite lattice spacing, they are generically heavier than the physical fermions, and they split into multiplets with different masses. Staggered fermions are the most common way to partially reduce the number of doublers. For each physical quark flavors, there are four in the Staggered formulation. Chiral symmetry is broken on the lattice, due to a flavor-mixing interaction at finite lattice spacing. However, at least a part of chiral symmetry is preserved in the case of staggered fermions. Wilson fermions were constructed by introducing a second-order derivative in the action, so that fermion doublers are removed in the limit $a \to 0$. However, the Wilson term is essentially the mass term for doublers, and for this reason chiral symmetry is violated even when the bare quark mass tends to zero. The numerical analysis of chiral properties is therefore much easier in the case of staggered fermions, and it requires less computer power as well. We will mainly report on results with staggered fermions in this manuscript.

The Matsubara formalism for finite temperature statistical systems is used to define QCD at finite temperature. The system under consideration is static, in thermal equilibrium, with a fixed temperature $T$. The partition function is given by:

$$Z(T,V) = \int \prod_\mu \mathcal{D}A_\mu \prod_f \mathcal{D}\psi_f \mathcal{D}\bar{\psi}_f \exp(-S_E(T,V)) \tag{1}$$

with

$$S_E(T,V) = -\int_0^{1/T} dx_4 \int_V d^3x \mathcal{L}^E,$$
$$\mathcal{L}^E = -\sum_f \bar{\psi}_f(x)(\not{\partial} + m_f)\psi_f(x) - \frac{1}{4}F^a_{\mu\nu}(x)F^{\mu\nu}_a(x) \tag{2}$$

and

$$\not{\partial} = (\partial_\mu + ig\frac{\lambda^a}{2}A^a_\mu)\gamma^E_\mu \qquad F^a_{\mu\nu} = \partial_\mu A^a_\nu - \partial_\nu A^a_\mu - gf^{abc}A^b_\mu A^c_\nu. \tag{3}$$

The thermodynamic quantities we are discussing are the pressure $p$, energy density $\epsilon$, entropy density $s$ and trace anomaly or interaction measure $I$. The latter vanishes for a massless, non-interacting gas. They are related to the partition function of the system through the following thermodynamic relationships:

$$\epsilon = \frac{T^2}{V}\left.\frac{\partial \ln Z(V,T)}{\partial T}\right|_V \qquad p = \left.\frac{T\partial \ln Z(V,T)}{\partial V}\right|_T$$
$$I = \epsilon - 3p \qquad s = \frac{\epsilon + p}{T} \qquad c_s^2 = \frac{\mathrm{d}p}{\mathrm{d}\epsilon}, \tag{4}$$

where $c_s^2$ is the speed of sound squared. We will calculate the thermal expectation value of physical observables $\mathcal{O}$ through the following expression

$$\langle \mathcal{O} \rangle = \frac{1}{Z(T,V)}\int \prod_\mu \mathcal{D}A_\mu \prod_f \mathcal{D}\psi_f \mathcal{D}\bar{\psi}_f \mathcal{O} \exp(-S_E(T,V)). \tag{5}$$

All of the above quantities can in principle depend also on the quark chemical potentials $\mu_f$. However, the fermion sign problem prevents the numerical calculation of these quantities at $\mu_f \neq 0$. One can try to circumvent this problem through analytical continuation of results obtained at finite imaginary chemical potential, where the sign problem is absent. We briefly explain this method here, as it will be useful for our discussion of results at finite density. A chemical potential $\mu$ can be introduced through weighted temporal links in the staggered formalism:

$$U_0(\mu) = e^{\mu}U_0, \qquad U_0^\dagger(\mu) = e^{-\mu}U_0^\dagger. \tag{6}$$

Therefore, an imaginary $\mu$ acts as a phase factor for the antiperiodic boundary condition in the Dirac operator. The $Z(3)$ symmetry of the gauge sector gives rise to a non-trivial periodicity in the imaginary chemical potential $\mu_f \to \mu_f + i(2\pi/3)T$, which is transferred to the baryochemical potential as $\mu_B \to \mu_B + i2\pi T$. This is the so-called Roberge–Weiss symmetry, which is independent of the charge conjugation symmetry $\mu_B \leftrightarrow -\mu_B$.

Introducing an imaginary chemical potential does not break the $\gamma_5$-Hermiticity of the Dirac operator. The imaginary chemical potential can simply be introduced as a phase shift in the time-like boundaries, and it can be implemented on a flavor-by-flavor basis. One can then make choices for the values of the chemical potentials $\mu_f$. Usually, $\mu_u = \mu_d$, while for the strange flavor different possibilities arise. A non-trivial choice is the tuning to $\langle n_S \rangle = 0$, which is the strangeness-neutral condition occurring in a heavy-ion collision. Imposing this condition on the lattice requires solving a differential equation, where the $\mu_S^I(\mu_B^I)$ function is to be determined:

$$\frac{d}{d\mu_B^I}\frac{\partial \log Z}{\partial \mu_S} = 0\,, \tag{7}$$

with the trivial initial condition $\partial \ln Z/\partial \mu_S = 0$ at $\mu_B^I = 0$.

## 3. QCD equation of state at $\mu_B = 0$

Once the lattice action is defined, the finite temperature lattice QCD formalism can be extended to the numerical evaluation of the Equation of State (EoS) of QCD. We start from QCD in the pure gauge case, to illustrate the method. This corresponds to a system in which only gluons are dynamical degrees of freedom, while quarks are too heavy to contribute to the thermodynamics. The partition function in this case is given by

$$Z(V,T) = \int DU e^{-S_G[U]}. \tag{8}$$

The two most common methods to calculate the EoS of QCD are the differential and the integral methods. Below I review the integral method, while the differential one is described in Appendix.

### 3.1. Integral method

The integral method is defined on an isotropic lattice ($a_s = a_t = a$) and uses the fact that, for a homogeneous system, the following expression for the pressure holds

$$p = \frac{T}{V} \ln Z(T, V). \tag{9}$$

For this reason, evaluating the pressure is equivalent to evaluating the partition function $Z$. For $\xi = 1$, the Wilson action becomes

$$S_G[U] = N_s^3 N_t \beta \left[P_s + P_t\right], \quad \text{with} \quad \beta = 2\frac{N_c}{g^2} \quad \text{and} \quad g_s = g_t = g, \tag{10}$$

and we can easily get

$$\ln Z|_\beta - \ln Z|_{\beta_0} = -N_s^3 N_t \int_{\beta_0}^{\beta} d\beta' \left[\langle P_s(\beta')\rangle + \langle P_t(\beta')\rangle\right]. \tag{11}$$

This procedure yields the pressure up to an additive constant

$$\left.\frac{p}{T^4}\right|_\beta - \left.\frac{p}{T^4}\right|_{\beta_0} = -N_t^4 \int_{\beta_0}^{\beta} d\beta' \left[\langle P_s(\beta')\rangle + \langle P_t(\beta')\rangle\right]. \tag{12}$$

The additive constant is usually chosen to be zero at some value of $\beta_0$ corresponding to a small temperature $T \leq T_0$. This is because, below $T \simeq 200$ MeV, the pressure $p \sim \exp[-m_g/T]$ is dominated by the lightest glueball states, which have a mass $m_g \sim 1$ GeV. Therefore, the pressure is small for $T \leq T_0$. With this choice and the usual vacuum subtraction, we get

$$\frac{p(\beta)}{T^4} = -N_t^4 \int_{\beta_0}^{\beta} d\beta' \left[D_s(\beta') + D_t(\beta')\right]. \tag{13}$$

One can obtain the other observables from the pressure, through thermodynamic identities

$$\begin{aligned} \left.\frac{\partial p}{\partial T}\right|_V &= \left.\frac{\partial S}{\partial V}\right|_T = s = \frac{\epsilon + p}{T} \\ \frac{\Delta I}{T^4} &= \frac{\epsilon - 3p}{T^4} = T \left.\frac{\partial (p/T^4)}{\partial T}\right|_V . \end{aligned} \tag{14}$$

For an isotropic lattice the following relationships hold

$$T = \frac{1}{N_t a}; \qquad \frac{\partial}{\partial T} = \frac{\partial a}{\partial T}\frac{\partial}{\partial a} = -\frac{1}{N_t T^2}\frac{\partial}{\partial a} = -\frac{N_t^2 a^2}{N_t}\frac{\partial}{\partial a} \tag{15}$$

so that

$$T \left.\frac{\partial}{\partial T}\right|_V = -a\frac{\partial}{\partial a}. \tag{16}$$

One can easily verify that

$$\frac{\Delta I}{T^4} = N_t^4 \left(a\frac{\partial \beta}{\partial a}\right)\left[D_s + D_t\right] = 2N_c N_t^4 \frac{B}{2\pi\alpha_s^2}\left[D_s + D_t\right]. \tag{17}$$

We can use a non-perturbative $\beta$-function for $B(\alpha_s)$. High precision results for the pure-glue trace anomaly in QCD are shown in the left panel of Fig. 1. The right panel shows a comparison with the trace anomaly obtained within the glueball resonance model, calculated using the twelve lightest glueballs [20].

If the system contains dynamical quarks, one can take other derivatives of the pressure with respect to the bare parameters of the action

$$p^{lat}(\beta, m_f) - p^{lat}(\beta_0, m_{f0}) = \frac{1}{N_t N_s^3} \int_{\beta_0, m_{f0}}^{\beta, m_f} \left[d\beta \frac{\partial \ln Z}{\partial \beta} + \sum_f dm_f \frac{\partial \ln Z}{\partial m_f}\right]. \tag{18}$$

One can show that

$$\begin{aligned} \langle -S_G\rangle &= \frac{1}{N_t N_s^3}\frac{\partial \ln Z}{\partial \beta} \\ \langle \bar\psi_f \psi_f\rangle &= \frac{1}{N_t N_s^3}\frac{\partial \ln Z}{\partial m_f}, \end{aligned} \tag{19}$$

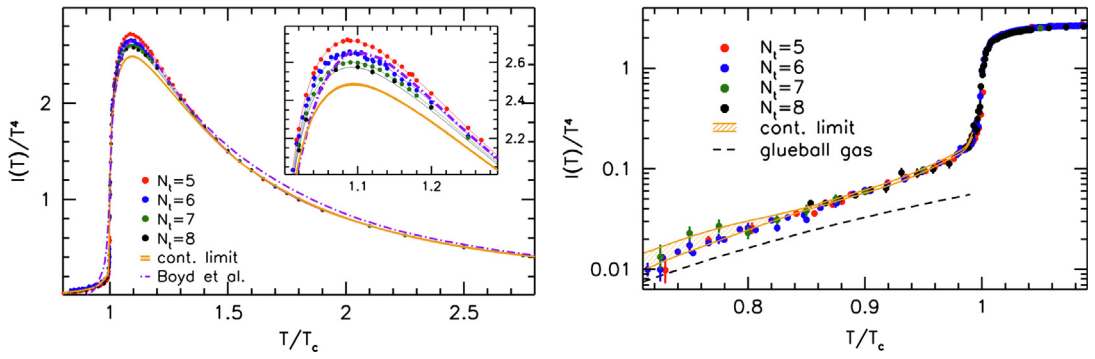


**Fig. 1.** From Ref. [20]. Left: the interaction measure on $N_s/N_t = 8$ lattices, for various lattice spacings and values of the temperature near the transition region. Right: the interaction measure in the confined phase, calculated at various lattice spacings. The yellow band shows the continuum extrapolation. In both panels, lattice QCD results correspond to a purely gluonic system. The dashed line corresponds to the glueball resonance model, in which the twelve lightest glueballs were introduced.

where the second quantity is the chiral condensate of flavor $f$. Subtracting the vacuum contribution one gets

$$\begin{aligned} \langle S_G\rangle^{sub} &= \langle S_G\rangle_{N_t,N_s} - \langle S_G\rangle_{N_t^{sub},N_s} \\ \langle \bar\psi_f\psi_f\rangle^{sub} &= \langle \bar\psi_f\psi_f\rangle_{N_t,N_s} - \langle \bar\psi_f\psi_f\rangle_{N_t^{sub},N_s} \end{aligned} \tag{20}$$

and it follows that

$$\frac{p(T)}{T^4} - \frac{p(T_0)}{T_0^4} = N_t^4 \int_{(\beta_0,m_{f0})}^{(\beta,m_f)} \left[ d\beta \langle -S_G\rangle^{sub} + \sum_f dm_f \langle \bar\psi_f\psi_f\rangle^{sub} \right]. \tag{21}$$

In Ref. [21] it was noticed that $\langle -S_G\rangle^{sub}$ decreases as $(N_t)^{-4}$, while $\langle \bar\psi_f\psi_f\rangle^{sub}$ only decreases as $(N_t)^{-2}$. Thus, the term containing the gauge action has $(N_t)^2$ larger errors. The typical integral method consists of calculating the interaction measure for several temperatures, then integrating it to get the pressure up to an integration constant. The modified method sets the strange quark mass $m_s$ to its physical value and changes $R$ from 1 to the physical value of 28.15, where the light quark mass is $m_{u,d} = \frac{m_s}{R}$. One can then calculate the derivatives of the pressure at several values of $\beta$ and $R$:

$$\begin{aligned} D_\beta &= \left.\frac{\partial}{\partial\beta}\right|_R \frac{p}{T^4} = N_t^4 \left[ \langle -S_G\rangle^{sub} + \frac{\partial m_s^{phys}}{\partial\beta} \left( \langle \bar\psi_s\psi_s\rangle^{sub} + \frac{1}{R}\langle \bar\psi_{ud}\psi_{ud}\rangle^{sub} \right) \right] \\ D_R &= \left.\frac{\partial}{\partial R}\right|_\beta \frac{p}{T^4} = -N_t^4 \frac{m_s^{phys}}{R^2} \langle \bar\psi_{ud}\psi_{ud}\rangle^{sub}. \end{aligned} \tag{22}$$

We can consider different integration paths in the $(\beta, R)$ plane, as the integral of the total derivative only depends on the initial and final points. Fig. 2 shows an example of integration path.

### 3.2. High temperature, ideal gas limit

It is reasonable to attempt a perturbative expansion of the pressure at high energy density or temperature, since the effective QCD coupling tends to zero logarithmically at large momentum transfer. To zeroth-order in the coupling, the deconfined phase of QCD is an ideal gas of massless gluons and quarks. We can therefore immediately write down the pressure of such a system, in the most general way:

$$p_0 = \frac{T}{V} \ln Z \tag{23}$$

where

$$\ln Z = Vd \int \frac{d^3p}{(2\pi)^3} \ln\left(1 \pm e^{-\beta(|\vec p|-\mu)}\right)^{\pm 1} \tag{24}$$

where the "+" sign is for fermions, the "−" sign is for bosons, and $d$ indicates the number of degrees of freedom. In the specific case of QCD we have

$$\begin{aligned} p^{QCD} = &\frac{T}{V} Vd_g \int \frac{d^3p}{(2\pi)^3} \ln\left(\left(1 - e^{-\beta(|\vec p|)}\right)^{-1}\right) + \frac{T}{V} Vd_q \int \frac{d^3p}{(2\pi)^3} \ln\left(1 + e^{-\beta(|\vec p|-\mu)}\right) \\ &+ \frac{T}{V} Vd_{\bar q} \int \frac{d^3p}{(2\pi)^3} \ln\left(1 + e^{-\beta(|\vec p|+\mu)}\right), \end{aligned} \tag{25}$$

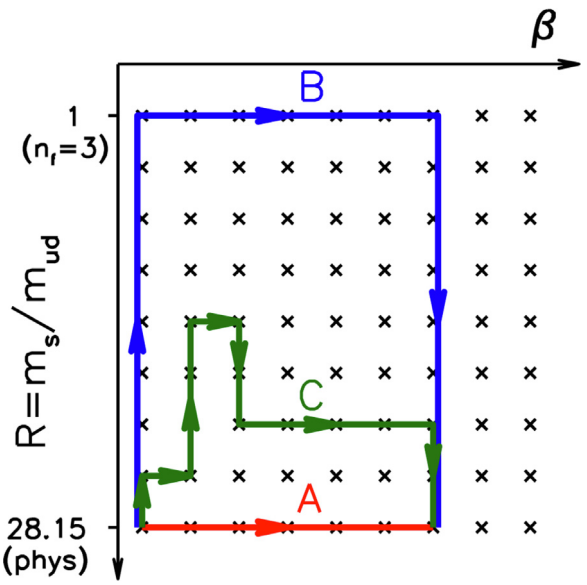


**Fig. 2.** From Ref. [21]. Example of possible integration paths for the pressure in the $(\beta, R)$ plane.

where $d_g = 2 \cdot (N_c^2 - 1) = 16$ (two possible polarizations times eight gluon colors) and $d_q = d_{\bar{q}} = 2 \cdot N_c = 6$. The gluon contribution is

$$\begin{aligned} p_g &= \frac{T}{V} V d_g \frac{4\pi}{(2\pi)^3} \int_0^\infty |\vec{p}|^2 d|\vec{p}| \ln\left[\frac{1}{1-e^{-\beta|\vec{p}|}}\right] \\ &= T d_g \frac{1}{2\pi^2} \frac{|\vec{p}|^3}{3} \ln\left[\frac{1}{1-e^{-\beta|\vec{p}|}}\right] + T^4 d_g \frac{1}{6\pi^2} \int_0^\infty \frac{|\vec{p}|^3}{T^3} \frac{d(|\vec{p}|/T)}{e^{|\vec{p}|/T}-1} \\ &= \frac{T^4 d_g}{6\pi^2} \frac{\pi^4}{15} = \frac{\pi^2 T^4}{90} d_g. \end{aligned} \tag{26}$$

The contribution of a quark of flavor $f$ is

$$\begin{aligned} p_f &= T^4 d_f \frac{4\pi}{(2\pi)^3} \int_0^\infty \frac{|\vec{p}|^3}{3T^3} \left[\frac{d(|\vec{p}|/T)}{e^{\beta(|\vec{p}|-\mu)}} + \frac{d(|\vec{p}|/T)}{e^{\beta(|\vec{p}|+\mu)}}\right] \\ &= \frac{d_f}{6\pi^2} \left[\frac{7\pi^4 T^4}{60} + \frac{\mu_f^2 \pi^2 T^2}{2} + \frac{\mu_f^4}{4}\right]. \end{aligned} \tag{27}$$

The total Stefan–Boltzmann limit for the QCD pressure thus follows as

$$p^{QCD} = \frac{\pi^2}{45} T^4 (N_c^2 - 1) + \sum_f \frac{N_c}{3\pi^2} \left[\frac{7\pi^4 T^4}{60} + \frac{\mu_f^2 \pi^2 T^2}{2} + \frac{\mu_f^4}{4}\right]. \tag{28}$$

In the limit $T \to \infty$, $\frac{p^{QCD}}{T^4}$ tends to a constant

$$\frac{p^{QCD}}{T^4} = \frac{8\pi^2}{45} + 7\frac{N_f \pi^2}{60}. \tag{29}$$

For $N_f = 3$ we have $\lim_{T\to\infty} \frac{p^{QCD}}{T^4} = 5.20896$.

Beyond the zeroth-order in the coupling, we can systematically construct a perturbative series and truncate it at a given order of the coupling constant. This has been a long-standing activity [22–28], which produced the pressure through order $g^6 \log g$ so far [29]. It turns out that the standard perturbative QCD series converges slowly: the left panel of Fig. 3 shows the total pressure calculated at different orders in the coupling, divided by the ideal gas limit value. The various truncations oscillate widely and show no signs of convergence in the shown temperature range. A reorganization of the perturbation series for thermal QCD was devised, called Hard Thermal Loop (HTL) [30–46], which systematically shifts the perturbative expansion from around an ideal gas of massless particles to around a gas of massive quasiparticles. The right panel of Fig. 3 shows the pressure, calculated at three-loop HTL order. It is clear that this technique brings the agreement between lattice and perturbative QCD down to lower temperature.

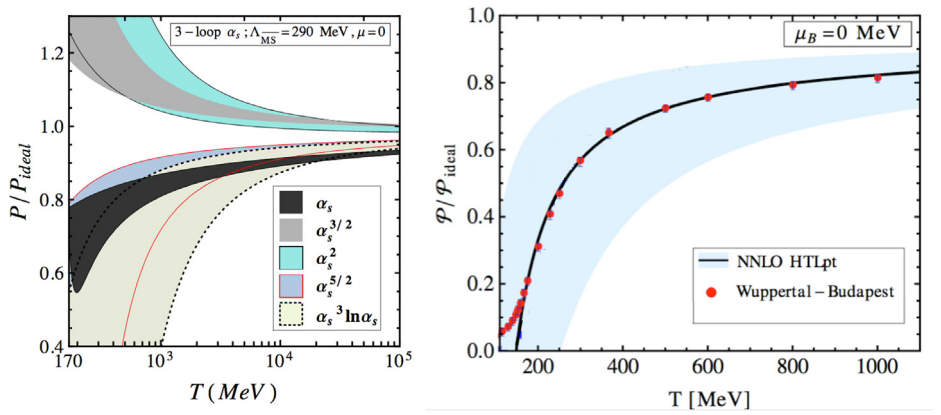


**Fig. 3.** Left: from Ref. [45]. Weak-coupling expansion for the scaled QCD pressure with $N_f = 3$. Shaded bands show the result of varying the renormalization scale $\mu$ by a factor of 2 around $\mu = 2\pi T$. Right: modified from Ref. [47]. Three-loop HTL perturbative resummation of the QCD pressure as a function of the temperature (shaded band). The pressure is rescaled by the ideal gas limit value. The perturbative results are compared to lattice QCD data from the WB [21] collaboration (red dots).

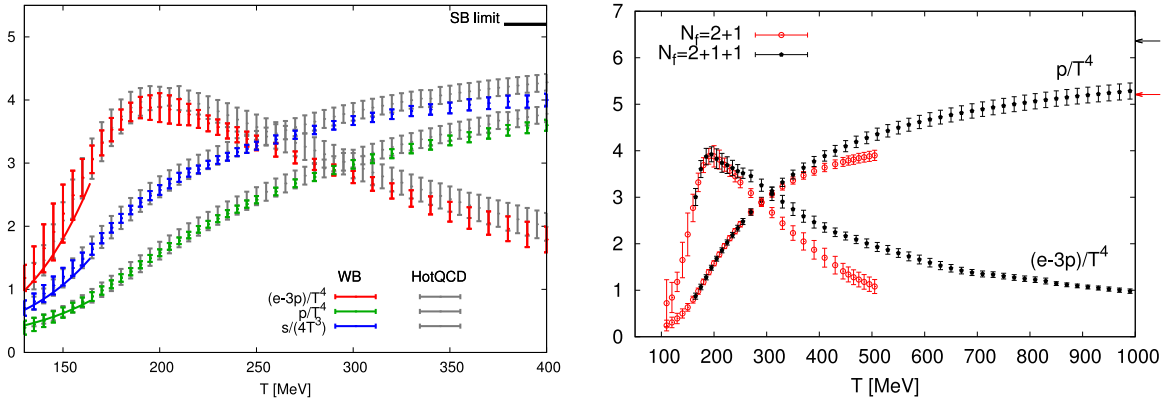


**Fig. 4.** Left: continuum extrapolated results for scaled interaction measure, entropy density and pressure as functions of the temperature. The colored points are from the WB collaboration [48], while the gray ones correspond to the HotQCD collaboration results [50]. The horizontal line at high temperature indicates the Stefan–Boltzmann limit for the pressure and the scaled entropy. The curves at low temperature are the predictions from the Hadron Resonance Gas (HRG) model. Right: pressure and interaction measure in the 2 + 1 (red) and 2 + 1 + 1 (black) flavor theories (from Ref. [52]).

### 3.3. Results

First principle results are available for the Equation of State of QCD with 2 +1 dynamical quark flavors with physical masses. Continuum extrapolated results for pressure, energy density, entropy density, speed of sound and interaction measure as functions of the temperature were published by the Wuppertal Budapest (WB) collaboration [21,48] using a tree-level Symanzik improved gauge, and stout-improved staggered fermion action with two levels of smearing (2stout) [49]. These results were later reproduced by the HotQCD collaboration [50] using the highly improved staggered quark (HISQ) action introduced in [51], a different staggered fermion discretization. The fact that two independent calculations, performed with different discretized versions of the QCD action, produce compatible results in the continuum limit is a crucial test of the theory. The left panel of Fig. 4 shows trace anomaly, pressure and entropy as functions of the temperature. Each observable is scaled by a power of the temperature, to make them dimensionless. The colored points correspond to the WB collaboration results, while the gray points correspond to results from the HotQCD collaboration. The horizontal line at high temperatures indicates the Stefan–Boltzmann limit for pressure and scaled entropy.

It is interesting to notice that some observables show a good agreement with resummation [37] or dimensional reduction [53] predictions already at $T \sim 400$ MeV, while for others this is not the case. For example, in the case of the interaction measure, the results from HTL perturbation theory at three-loop order [37] are affected by a large uncertainty, corresponding to a change in the renormalization scale. The results from Electrostatic QCD agree with the HTL ones, and the lattice points approach the perturbative results at $T \sim 2 - 3T_c$.

Simulations with other kinds of fermions, such as Wilson, overlap or domain wall, are typically more time-consuming. For this reason, results for the Equation of State of strongly interacting matter in these formulations are not yet available

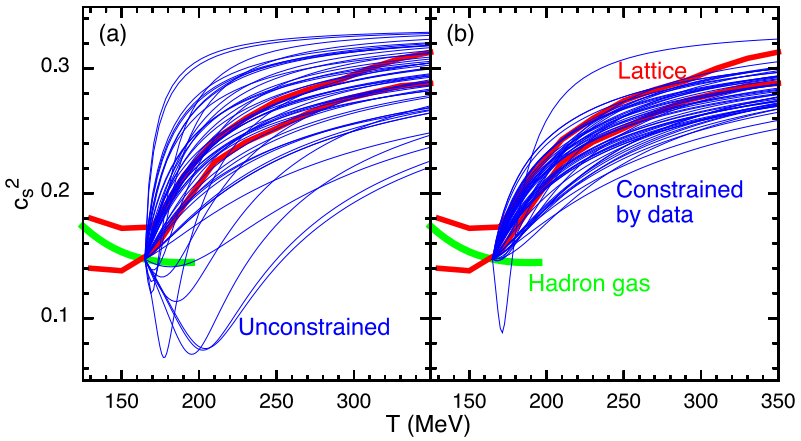


**Fig. 5.** From Ref. [57]. The two panels show how the Bayesian analysis constrains the QCD equation of state. (a) Fifty equations of state were generated through a random parameter choice from the prior distribution, and weighted by the posterior likelihood. (b) The two red lines in each figure show the lattice equation of state from [50], while the green line is the EOS for a non-interacting Hadron Resonance Gas.

with realistic parameters. Recently, other approaches to lattice QCD are generating first result for the Equation of State. These include the gradient flow method [54,55], which is based on extracting the thermodynamics from the energy–momentum tensor, and twisted mass fermions [56]. So far, the former are limited to the quenched approximation [54] or heavier-than-physical quark masses [55], the latter to two quark flavors with heavier-than-physical quark masses.

Results on the equation of state with $2+1+1$ dynamical flavors, including the charm quark, have recently become available [52]. They are shown in the right panel of Fig. 4. The figure clearly shows that the charm quark gives a non-negligible contribution to the thermodynamics already at $T \sim 250$ MeV. The effect of an EoS with charm on hydrodynamic simulations of heavy ion collisions at the LHC energies was recently investigated in Ref. [58].

Recently, the lattice QCD Equation of State has received an important validation from a Bayesian analysis [57]. This framework has applied state-of-the-art statistical techniques to the combined analysis of a large number of observables while varying the model parameters, in order to obtain a systematic comparison of data from RHIC and the LHC to theoretical models. The posterior distribution over possible equations of states is consistent with results from lattice QCD simulations, as shown in Fig. 5. This analysis was successfully applied to infer the behavior of other quantities, such as the shear viscosity of the system created in heavy-ion collisions at zero [59] and finite density [60].

## 4. Equation of state at finite chemical potential

### 4.1. Fermionic sign problem

A finite chemical potential $\mu$ is introduced in the fermionic part of the QCD action in the following way

$$S = \int_0^\beta d\tau \int d^3x \bar{\psi} \left[\gamma_\mu D^\mu + \mu\gamma_4 + m\right] \psi = \int d^4x \bar{\psi} M \psi, \tag{30}$$

namely as the imaginary part of the fourth-component of an abelian vector field. Due to this chemical potential, the QCD action becomes complex. This can be seen by the absence of $\gamma_5$ hermiticity. At vanishing chemical potential we have

$$(\gamma_5 M)^\dagger = \gamma_5 M, \tag{31}$$

which leads to the identity $M^\dagger = \gamma_5 M \gamma_5$ and, as a consequence, to

$$\det(M^\dagger) = \det(\gamma_5 M \gamma_5) = \det M = (\det M)^* . \tag{32}$$

When $\mu \neq 0$ we find

$$M^\dagger(\mu) = \gamma_5 M(-\mu^*)\gamma_5, \tag{33}$$

resulting in

$$[\det M(\mu)]^* = \det\left[M(-\mu^*)\right] \tag{34}$$

which is in general a complex number. In particular, for real $\mu$ we get

$$[\det M(\mu)]^* = \det\left[M(-\mu)\right] \tag{35}$$

while for imaginary $\mu$ we get

$$[\det M(\mu)]^* = \det [M(\mu)] \tag{36}$$

which is a real number. For this reason, simulations at imaginary chemical potential can be performed as they do not generate a sign problem. However, when the chemical potential is real, the QCD action becomes complex and cannot be used as a weight in the Monte Carlo sampling techniques used in lattice QCD simulations.

### 4.2. Thermodynamics at finite chemical potential

The equation of state of QCD at finite density is a very important quantity. In fact, it can be used to shed light on the matter created in ultrarelativistic heavy-ion collisions at low collision energies, or the core of compact stellar objects, or neutron star mergers. The latter cover a range of temperature and chemical potential which overlaps with the one reached by the lowest collision energies in heavy-ion experiments. Results from perturbative QCD at extreme density have been obtained, and used to study strongly interacting matter in the core of neutron stars [61–64]. The densities needed for perturbation theory to be valid are presumably very far away from the QCD transition line, hence the need for non-perturbative techniques. Unfortunately, the equation of state from first principles is currently only available in a limited range of chemical potentials, which will be discussed below.

The identities between thermodynamic quantities at finite chemical potential become

$$\begin{aligned} s(T,\mu_B) &= \left.\frac{\partial p}{\partial T}\right|_{\mu_B}, \qquad & n_B(T,\mu_B) &= \chi_1^B = \left.\frac{\partial p}{\partial \mu_B}\right|_T, \\ \epsilon(T,\mu_B) &= Ts - p + \mu_B n_B, \qquad & c_s^2(T,\mu_B) &= \left.\frac{\partial p}{\partial \epsilon}\right|_{s/n_B}, \end{aligned} \tag{37}$$

where $s$ is the entropy density, $p$ the pressure, $\epsilon$ the energy density, $n_B$ the baryonic density and $c_s^2$ the speed of sound squared.

The methods that have been proposed to solve QCD at finite $\mu_B$ include finding appropriate dual variables [65–78], using Lefschetz thimbles [79–86] or complex Langevin equation [87–106]. Unfortunately, none of them has produced quantitatively reliable results so far. At the moment, quantitatively significant results are obtained through two main methods, the Taylor expansion of thermodynamic quantities in powers of $\mu_B/T$ [107–111] or their simulation at imaginary chemical potentials followed by an analytical continuation to real $\mu_B$ [112–119]. A novel expansion method, introduced in Ref. [19], will be discussed in Section 4.7. Other methods have also been employed, e.g. reweighting of the generated configurations [120–123], canonical ensemble simulations [124–126] and density of state methods [127–136], but here I will focus on the first two.

### 4.3. Taylor expansion

We can write the pressure of QCD as a Taylor series in powers of $\mu_B/T$ around $\mu_B = 0$ in the following way:

$$\frac{p(T,\mu_B)}{T^4} = \frac{p(T,0)}{T^4} + \sum_{n=1}^{\infty} \frac{1}{n!} \left.\frac{\partial^n (p/T^4)}{\partial (\frac{\mu_B}{T})^n}\right|_{\mu_B=0} \left(\frac{\mu_B}{T}\right)^n = \sum_{n=0}^{\infty} c_n(T) \left(\frac{\mu_B}{T}\right)^n, \tag{38}$$

where the Taylor coefficients $c_n$ are defined as

$$c_n = \frac{1}{n!} \left.\frac{\partial^n (p/T^4)}{\partial (\mu_B/T)^n}\right|_{\mu_B=0}. \tag{39}$$

On the lattice, these coefficients are usually calculated in terms of the quark chemical potentials. A change of basis can then be performed through the following relationships:

$$\begin{aligned} \mu_u &= \frac{1}{3}\mu_B + \frac{2}{3}\mu_Q \\ \mu_d &= \frac{1}{3}\mu_B - \frac{1}{3}\mu_Q \\ \mu_s &= \frac{1}{3}\mu_B - \frac{1}{3}\mu_Q - \mu_S, \end{aligned} \tag{40}$$

so that

$$\begin{aligned} \frac{\partial}{\partial \mu_B} &= \frac{1}{3}\partial_u + \frac{1}{3}\partial_d + \frac{1}{3}\partial_s \\ \frac{\partial}{\partial \mu_Q} &= \frac{2}{3}\partial_u - \frac{1}{3}\partial_d - \frac{1}{3}\partial_s \end{aligned}$$

$$\frac{\partial}{\partial \mu_S} = -\partial_s. \tag{41}$$

In the above equations, we introduced the notation $\partial_i = \frac{\partial}{\partial \mu_i}$ to indicate the derivative with respect to the chemical potential of quark flavor $i$.

The coefficients $c_n$ can be in principle calculated on the lattice, since they are defined strictly at $\mu_B = 0$. However, the calculation of the higher order coefficients turns out to be very noisy, and therefore computationally expensive. We recall that $p = T \left.\frac{\partial \ln Z}{\partial V}\right|_T$ and that the partition function can be written as

$$Z = \int DU\, (detM)^{N_f}\, e^{-S_G[U]} = \int DU e^{-S_G[U]} e^{N_f \ln\det M(\mu)} \tag{42}$$

from which follows

$$\frac{\partial \ln Z}{\partial \mu} = \frac{\int DU e^{-S_G[U]} e^{N_f \ln\det M(\mu)}}{Z} N_f \frac{\partial[\ln\det M(\mu)]}{\partial \mu} = \left\langle N_f \frac{\partial \ln\det M(\mu)}{\partial \mu} \right\rangle. \tag{43}$$

Higher order derivatives can then be taken in a similar fashion. For example, for the second-order one we have

$$\begin{aligned}
\frac{\partial^2 \ln Z}{\partial \mu^2} &= \frac{\partial}{\partial \mu}\left[\frac{\int DU e^{-S_G[U]} e^{N_f \ln\det M(\mu)}}{Z} N_f \frac{\partial[\ln\det M(\mu)]}{\partial \mu}\right] \\
&= \frac{\int DU e^{-S_G[U]} e^{N_f \ln\det M(\mu)}}{Z} \left(N_f \frac{\partial[\ln\det M(\mu)]}{\partial \mu}\right)^2 \\
&+ \frac{\int DU e^{-S_G[U]} e^{N_f \ln\det M(\mu)}}{Z} N_f \frac{\partial^2[\ln\det M(\mu)]}{\partial \mu^2} \\
&- \frac{1}{Z^2} \int DU e^{-S_G[U]} e^{N_f \ln\det M(\mu)} N_f \frac{\partial[\ln\det M(\mu)]}{\partial \mu} \\
&\times \int DU e^{-S_G[U]} e^{N_f \ln\det M(\mu)} N_f \frac{\partial[\ln\det M(\mu)]}{\partial \mu} \\
&= \left\langle N_f \frac{\partial^2 \ln\det M(\mu)}{\partial \mu^2} \right\rangle + \left\langle \left(N_f \frac{\partial \ln\det M(\mu)}{\partial \mu}\right)^2 \right\rangle - \left\langle N_f \frac{\partial \ln\det M(\mu)}{\partial \mu} \right\rangle^2
\end{aligned} \tag{44}$$

and so on. Writing $\ln\det M = tr \ln M$, we can express these as

$$\begin{aligned}
\frac{\partial}{\partial \mu} \ln\det M &= trM^{-1} \frac{\partial M}{\partial \mu}; \\
\frac{\partial^2}{\partial \mu^2} \ln\det M &= trM^{-1} \frac{\partial^2 M}{\partial \mu^2} - trM^{-1} \frac{\partial M}{\partial \mu} M^{-1} \frac{\partial M}{\partial \mu}.
\end{aligned} \tag{45}$$

We introduce new quantities $\chi_n^i$, which are related to these coefficients as

$$c_n^i = \frac{1}{n!} \chi_n^i, \quad \text{where} \quad \chi_n^{\ i} = \frac{\partial^n (p/T^4)}{\partial (\mu_i/T)^n}. \tag{46}$$

The $\chi_n^i$ are called susceptibilities of conserved charges (or quark flavors) and have an important physical interpretation. The first-order up quark susceptibility

$$\chi_1^u = \frac{\partial (p/T^4)}{\partial (\mu_u/T)} = \frac{1}{T^3} n_u \tag{47}$$

is the density of $u$ quarks, while the second-order one

$$\chi_2^u = \frac{\partial}{\partial (\mu_u/T)} \left(\frac{n_u}{T^3}\right) \tag{48}$$

measures the response of the up quark density to an infinitesimal change in the up quark chemical potential. The non-diagonal second-order susceptibility

$$\chi_{11}^{us} = \frac{\partial}{\partial (\mu_s/T)} \left(\frac{n_u}{T^3}\right) \tag{49}$$

measures the response of the up quark density to an infinitesimal change in the strange quark chemical potential, namely it measures the up and strange quark correlations.

Susceptibilities of conserved charges are derivatives of the scaled pressure $(p/T^4)$ with respect to the scaled chemical potential $\mu_B/T$. For this reason, they share the same Taylor expansion coefficients as the pressure, with different numerical

factors. This can be seen from the following equations, which show the first few terms in the expansion of the scaled pressure, $\chi_1$, $\chi_2$, $\chi_3$

$$\begin{aligned}
\frac{p(T,\ \mu_B)}{T^4} &= p(T,\ \mu_B=0) + c_2(T)\left(\frac{\mu_B}{T}\right)^2 + c_4(T)\left(\frac{\mu_B}{T}\right)^4 + c_6(T)\left(\frac{\mu_B}{T}\right)^6 + \cdots \\
\frac{T\chi_1(T,\ \mu_B)}{\mu_B} &= 2c_2(T) + 4c_4(T)\left(\frac{\mu_B}{T}\right)^2 + 6c_6(T)\left(\frac{\mu_B}{T}\right)^4 + \cdots \\
\chi_2(T,\ \mu_B) &= 2c_2(T) + 12c_4(T)\left(\frac{\mu_B}{T}\right)^2 + 30c_6(T)\left(\frac{\mu_B}{T}\right)^4 + \cdots \\
\frac{T\chi_3(T,\ \mu_B)}{\mu_B} &= 24c_4(T) + 120c_6(T)\left(\frac{\mu_B}{T}\right)^2 + \cdots\ .
\end{aligned} \tag{50}$$

For this reason, if we obtain the first few coefficients $c_i$, we will be able to extrapolate both the pressure and the susceptibilities to finite $\mu_B$. It is important to mention that, since QCD is symmetric with respect to a change of sign in chemical potential, these observables are all even functions of $\mu_B$ and all odd coefficients are therefore vanishing at $\mu_B = 0$.

### 4.4. Simulations at imaginary chemical potential

#### 4.4.1. Simulation setup

We have seen that the higher order coefficients appear in the Taylor series of the lower order ones in power of $\mu_B/T$ (see Eqs. (50)). Thus, it is possible to determine them more precisely through simulations at imaginary chemical potential, compared to what can be achieved with the direct simulation method. At imaginary $\mu_B$, $\mu_B^2$ and $\mu_B^6$ will be negative in Eqs. (50). One can perform a fit of these lower-order coefficients at finite, imaginary $\mu_B$. The coefficients of the fit, namely $c_2(T)$, $c_4(T)$ and $c_6(T)$, can be extracted in this way. Values for $\mu_S$ and $\mu_Q$ must be chosen to perform these simulations (or equivalently, values for $\mu_d$ and $\mu_s$). At $\mu_B = 0$ this is not an issue, as in that case one usually sets $\mu_S = 0$ and $\mu_Q = 0$.

The two main choices when simulating at finite imaginary $\mu_B$ are to either set $\mu_S = 0$ and $\mu_Q = 0$, or to fix them to match the experimental situation in a heavy-ion collision, namely

$$\begin{aligned}
\langle n_S\rangle &= 0 \\
\langle n_Q\rangle &= 0.4\langle n_B\rangle .
\end{aligned} \tag{51}$$

These two relationships stem from the initial conditions of the ions being collided in the accelerator, which do not contain any valence strange quark and for which the number of protons is approximately 0.4 times the atomic number. The first condition gives rise to a differential equation

$$\langle n_S\rangle = 0 \quad \leftrightarrow \quad \left\langle \frac{\partial \ln Z}{\partial \mu_S}\right\rangle = 0 \tag{52}$$

from which, deriving with respect to $\mu_B$, we can obtain a relationship between $\mu_S$, $\mu_B$ and $T$:

$$\frac{d}{d\mu_B}\left[\frac{\partial \ln Z}{\partial \mu_S}\right] = \frac{\partial^2 \ln Z}{\partial \mu_S \partial \mu_B} + \frac{\partial^2 \ln Z}{\partial \mu_S^2}\frac{\partial \mu_S}{\partial \mu_B} = 0, \tag{53}$$

namely

$$\frac{\partial \mu_S}{\partial \mu_B} = -\frac{\chi_{11}^{BS}(T)}{\chi_2^S(T)} \tag{54}$$

to lowest order. Higher order conditions can be obtained by further deriving $\frac{\partial \ln Z}{\partial \mu_S}$ with respect to $\mu_B$. By solving these differential equations, we get the $\mu_S(\mu_B, T)$ that satisfies the desired conditions. The left panel of Fig. 6 shows an example of $\mu_S(T)$ for different values of $\mu_B/T$. The drawback of this method is that, for each value of the temperature, a different set of configurations needs to be generated with specific values of imaginary $\mu_B$ and $\mu_S$. The right panel of Fig. 6 shows different landscapes for simulations at imaginary $\mu_B$ and $\mu_S$. The black dot corresponds to direct simulation of all coefficients at $\mu_B = 0$. The red squares correspond to finite $\mu_B$ and $\mu_S = 0$, while the green triangles are trajectories which ensure the strangeness-neutrality condition at $T = 150$ MeV (full) and $T = 200$ MeV (empty).

In Ref. [138], the rescaled baryonic density $T\chi_1^B/\mu_B$ was fitted with three different functions:

$$\begin{aligned}
B_1(\hat{\mu}) &= a + b\hat{\mu}^2 + c\hat{\mu}^4 \\
B_2(\hat{\mu}) &= (a + b\hat{\mu}^2)/(1 + c\hat{\mu}^2) \\
B_3(\hat{\mu}) &= a + b\hat{\mu}^2 + c\,\sin(\hat{\mu})/\hat{\mu}.
\end{aligned} \tag{55}$$

These fits are shown in the left panel of Fig. 7.

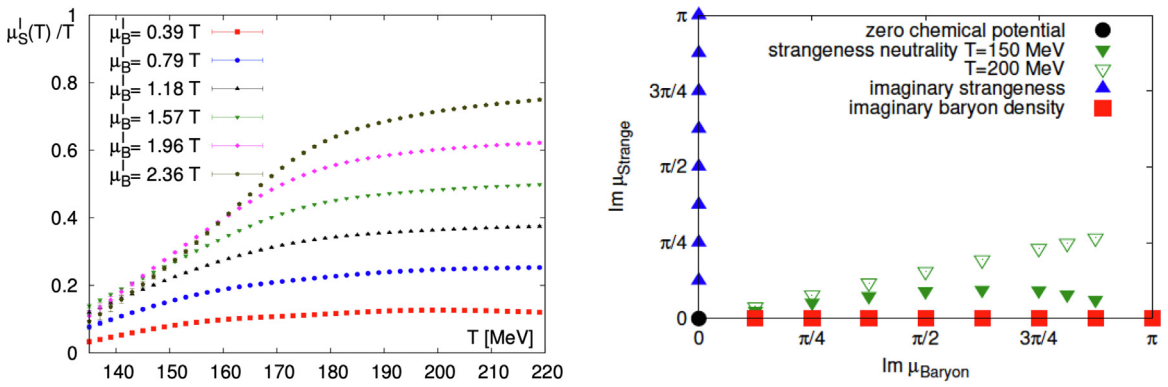


**Fig. 6.** Left: from Ref. [137]. Continuum extrapolated results for the imaginary strangeness chemical potentials that realize strangeness neutrality. Results are shown as functions of the temperature, for different values of imaginary $\mu_B/T$. Right: landscape of simulation points in the $(\Im(\mu_B), \Im(\mu_S))$ plane: the black circle corresponds to $\Im(\mu_B) = \Im(\mu_S) = 0$, the blue triangles to simulations at finite imaginary $\mu_S$ and zero baryon chemical potential, the red squares to simulations at finite imaginary $\mu_B$ and zero strangeness chemical potential. The two sets of green triangles correspond to simulations at finite $\Im(\mu_B)$ and $\Im(\mu_S)$ that satisfy the experimental constraints (51) at two different temperature values.

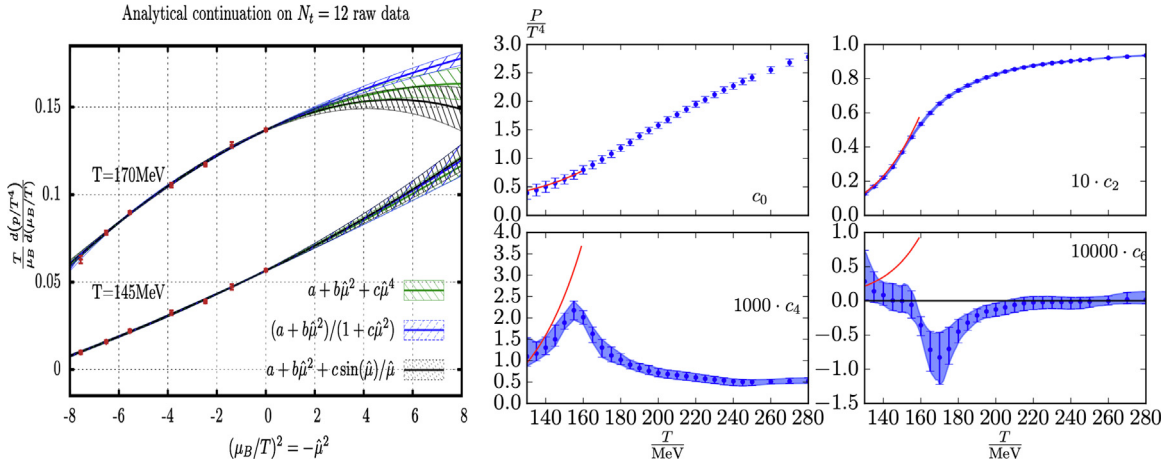


**Fig. 7.** From Ref. [138]. Left: analytical continuation of $T\chi_1^B/\mu_B$ from negative to positive $(\mu_B/T)^2$ for $T = 145$ MeV (lower curves) and $T = 170$ MeV (upper curves). The different colors correspond to different fitting functions. Right: continuum extrapolated coefficients $c_0 \ldots c_6$ for the Taylor expansion of the pressure around $\mu_B = 0$ as functions of the temperature, in comparison to the Hadron Resonance Gas model prediction (red lines). These coefficients correspond to the strangeness neutrality condition, in which $\mu_S$ and $\mu_Q$ are functions of $T$ and $\mu_B$ that match the experimental conditions in a heavy-ion collision.

More recently, the authors of Ref. [139] performed a new, combined fit of lower-order fluctuations up to order four. The formulas used for the combined fit of $\chi_1, \ldots \chi_4$ are

$$\begin{aligned}
\chi_1^B(\hat{\mu}_B) &= 2c_2\hat{\mu}_B + 4c_4\hat{\mu}_B^3 + 6c_6\hat{\mu}_B^5 + \frac{4!}{7!}c_4\epsilon_1\hat{\mu}_B^7 + \frac{4!}{9!}c_4\epsilon_2\hat{\mu}_B^9 \\
\chi_2^B(\hat{\mu}_B) &= 2c_2 + 12c_4\hat{\mu}_B^2 + 30c_6\hat{\mu}_B^4 + \frac{4!}{6!}c_4\epsilon_1\hat{\mu}_B^6 + \frac{4!}{8!}c_4\epsilon_2\hat{\mu}_B^8 \\
\chi_3^B(\hat{\mu}_B) &= 24c_4\hat{\mu}_B + 120c_6\hat{\mu}_B^3 + \frac{4!}{5!}c_4\epsilon_1\hat{\mu}_B^5 + \frac{4!}{7!}c_4\epsilon_2\hat{\mu}_B^7 \\
\chi_4^B(\hat{\mu}_B) &= 24c_4 + 360c_6\hat{\mu}_B^2 + c_4\epsilon_1\hat{\mu}_B^4 + \frac{4!}{6!}c_4\epsilon_2\hat{\mu}_B^6
\end{aligned} \tag{56}$$

where $\epsilon_1$ and $\epsilon_2$ are drawn randomly from a normal distribution with mean $-1.25$ and variance 2.75. This is done to eliminate the ambiguity coming from the fitting function and just assumes that $8!c_8 \leq 4!c_4$ and $10!c_{10} \leq 4!c_4$, or equivalently that $\chi_8^B \leq \chi_4^B$ and $\chi_{10}^B \leq \chi_4^B$.

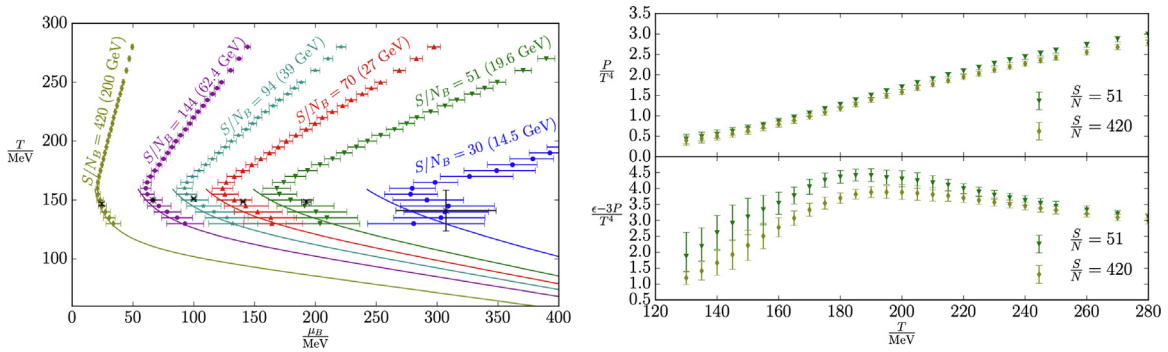


**Fig. 8.** From Ref. [138]. Left: isentropic trajectories in the $(T,\ \mu_B)$ plane: the contours are calculated at fixed $S/N_B$ values. The black points are the chemical freeze-out parameters from Ref. [142]. Right: pressure (top) and interaction measure (bottom) as functions of the temperature, calculated along the highest and lowest isentropic trajectories from the left panel.

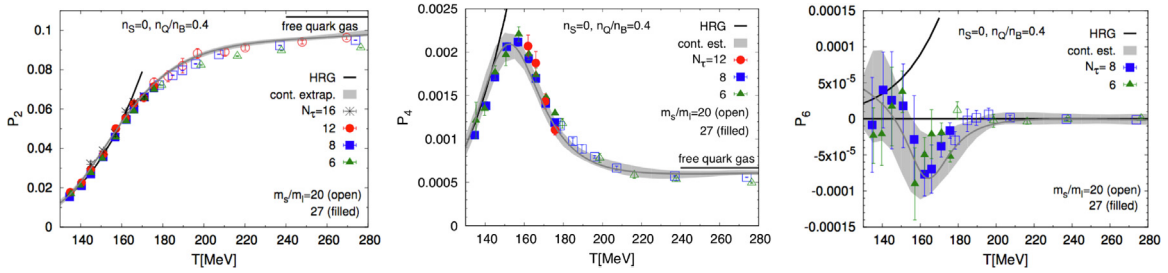


**Fig. 9.** From Ref. [144]. Expansion coefficients of the pressure as functions of the temperature in the case of strangeness neutrality. The broad gray bands show the continuum extrapolation. The curves at low temperature show the HRG model calculations based on resonances listed by the Particle Data Group.

### 4.5. Results

Early results for $c_2$, $c_4$ and $c_6$ were obtained in Ref. [108], while the first continuum extrapolated results for $c_2$ were published in Ref. [140]; in Ref. [141] $c_4$ was shown, but only at finite lattice spacing. The continuum limit for $c_6$ was published for the first time in [138] in the case of strangeness neutrality.

The Taylor coefficients from Ref. [138] are shown in the right panel of Fig. 7. From these coefficients, one can reconstruct the pressure at finite temperature and chemical potential, and from the pressure all other quantities can be obtained through the thermodynamic relationships listed in Eqs. (37).

The left panel of Fig. 8 displays the isentropic trajectories in the $(T, \mu_B)$-plane obtained in Ref. [138]. They correspond to the values of $T$ and $\mu_B$ at which the entropy per baryon takes a constant value, determined at the freeze-out points (in black) for each collision energy at RHIC. These trajectories would be followed by the system created in a heavy-ion collision in the case of a vanishing shear viscosity. It was however pointed out that the actual trajectories can be quite different, due to dissipative effects [143]. The right panel of Fig. 8 shows the pressure and interaction measure obtained along the highest and lowest trajectories. Results for $c_6$ were later published in Ref. [144], both in the case of strangeness neutrality and at $\mu_S = \mu_Q = 0$. The three panels of Fig. 9 show $c_2$, $c_4$ and $c_6$ in the case of strangeness neutrality (called $P_2$, $P_4$ and $P_6$ in Ref. [144]), while the three panels of Fig. 10 show $\chi_2^B$, $\chi_4^B/\chi_2^B$ and $\chi_6^B/\chi_2^B$ calculated at $\mu_S = \mu_Q = 0$.

Ref. [145] contains a first determination of $c_8$, at two values of the temperature and $N_t = 8$. More recently, diagonal and non-diagonal coefficients up to $c_8$ have been calculated at $N_t = 12$ in Ref. [139] at $\mu_S = \mu_Q = 0$. The diagonal ones are shown in Fig. 11.

Recently, the diagonal and off-diagonal coefficients from Ref. [139] have been used to construct a lattice-based equation of state at finite $\mu_B$, $\mu_S$ and $\mu_Q$ in Ref. [146] through the following Taylor expansion:

$$\frac{p(T,\mu_B,\mu_S,\mu_Q)}{T^4} = \sum_{i,j,k} \frac{1}{i!j!k!} \chi_{ijk}^{BQS} \left(\frac{\mu_B}{T}\right)^i \left(\frac{\mu_S}{T}\right)^j \left(\frac{\mu_Q}{T}\right)^k, \tag{57}$$

where

$$\chi_{ijk}^{BQS} = \frac{\partial^{i+j+k}(p/T^4)}{\partial(\frac{\mu_B}{T})^i \partial(\frac{\mu_Q}{T})^j \partial(\frac{\mu_S}{T})^k}. \tag{58}$$

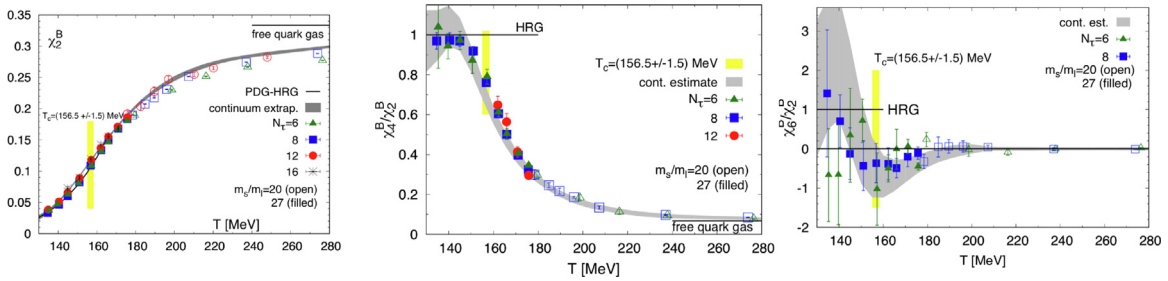


**Fig. 10.** From Ref. [144]. Expansion coefficients of the pressure as functions of the temperature in the case of $\mu_S = \mu_Q = 0$. The broad gray bands show the continuum extrapolation. The curves at low temperature show the HRG model calculations based on resonances listed by the Particle Data Group. Notice that, for the ratios $\chi_4^B/\chi_2^B$ and $\chi_6^B/\chi_2^B$, these ratios are flat in the ideal HRG model, independently of the particle spectrum considered as input.

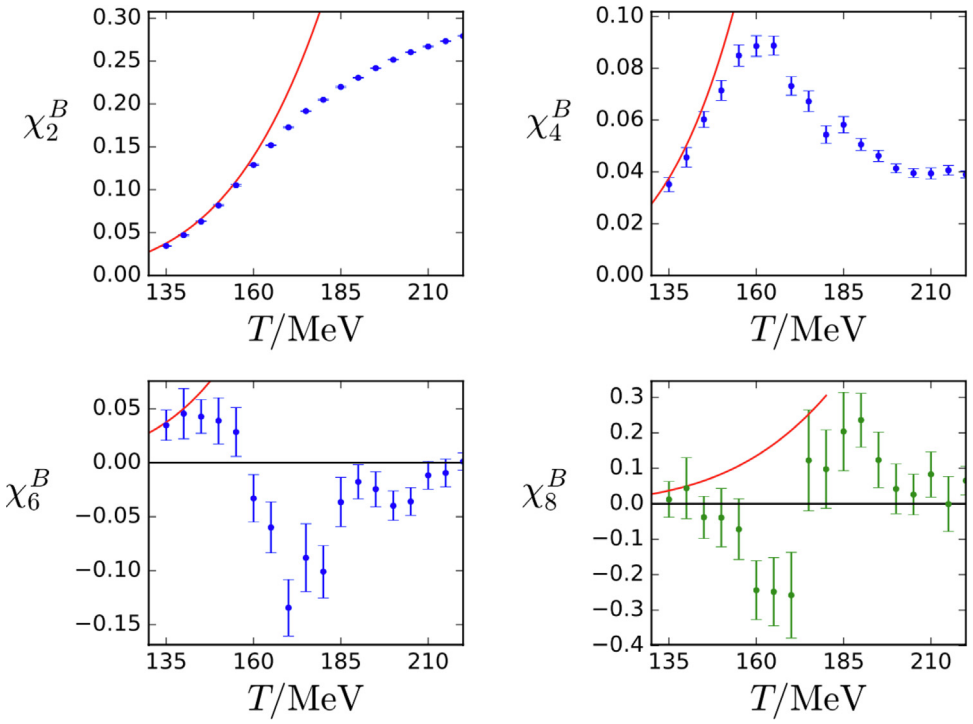


**Fig. 11.** From Ref. [139]. Expansion coefficients of the pressure as functions of the temperature at $\mu_S = \mu_Q = 0$, obtained at $N_t = 12$. $\chi_8^B$ is plotted in green to highlight that its determination is guided by a prior, that is linked to the $\chi_4^B$ observable.

This equation of state is very useful as, even if strangeness is globally conserved in heavy-ion collisions, the fluid cells in hydrodynamic simulations can have large local fluctuations that violate strangeness neutrality and electric charge conservation. Similar results were obtained in Ref. [147].

### *4.6. Resumming Taylor expansions*

Recently, the authors of Ref. [148] proposed a resummation of the Taylor series, which includes up to infinite powers of $\mu_B/T$. We will now see how this resummation is achieved. As we have seen above, the Taylor expansion of the excess pressure to order $\mathcal{O}(\mu_B^N)$ can be written as

$$\frac{P(T,\mu_B)}{T^4} - \frac{P(T,0)}{T^4} = \sum_{n=1}^{N} \frac{\chi_n^B}{n!} \left(\frac{\mu_B}{T}\right)^n , \tag{59}$$

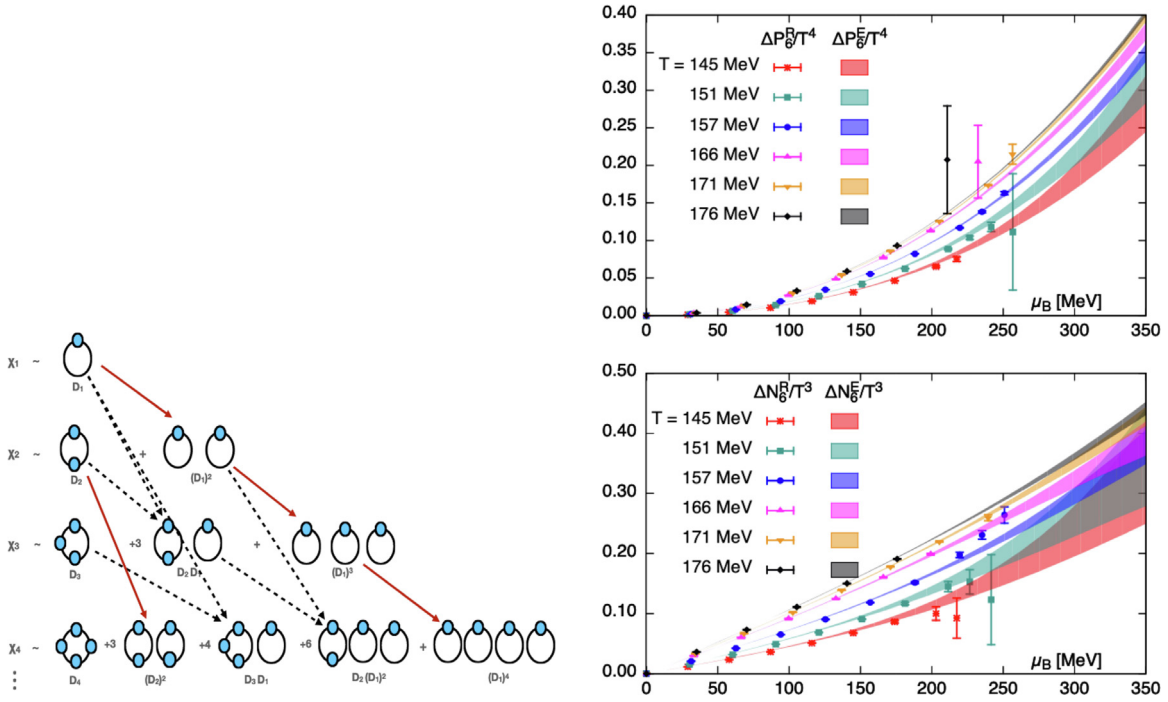


**Fig. 12.** From Ref. [148]. Left: Contributions of different $D_n$ to the $\chi_n^B$. Each blob represents insertion of the 0-th component of the conserved current. Solid red and dotted black lines represent exponentiated and cross terms, respectively. Right: comparison between Taylor and resummed excess pressure (top panel) and net-baryon density (bottom panel).

with Taylor coefficients defined as

$$\chi_n^B = \frac{1}{VT^3} \left. \frac{\partial^n \ln Z(T,\mu_B)}{\partial(\mu_B/T)^n} \right|_{\mu_B=0} . \tag{60}$$

In the above equation, $Z$ denotes the partition function of QCD and $V$ the spatial volume. As evident from Eq. (44), each $\chi_n^B$ contains the expectation values of product of terms like

$$D_n = \left. \frac{\partial^n \ln \det M(T,\mu_B)}{\partial(\mu_B/T)^n} \right|_{\mu_B=0} . \tag{61}$$

In the continuum, $D_n$ is the integrated $n-$point correlation function of the zeroth-component of the baryon current. Thus, lattice computations of $\chi_n^B$ involve the calculation of all $D_n$ and their powers.

It is not difficult to realize that, taking into account the factorials and the powers of $\mu_B/T$, all contributions of each $D_n$ to the excess pressure can be resummed into exponential forms (see the left panel of Fig. 12). Using this method, it is possible to write a resummed version of the equation of state

$$\frac{P(T,\mu_B)}{T^4} - \frac{P(T,0)}{T^4} = \frac{1}{VT^3} \ln\langle \exp\left[ \sum_{n=1}^{N} \frac{D_n}{n!} \left(\frac{\mu_B}{T}\right)^n \right] \rangle, \tag{62}$$

which contains infinite orders in $\mu_B$.

The right panels of Fig. 12 show a comparison between the Taylor expansion and its resummation for the excess pressure (top panel) and the net-baryon density (bottom panel) as functions of $\mu_B$ for different values of the temperature.

### 4.7. A novel expansion scheme

#### 4.7.1. Motivation

As we have seen in the above Sections, correlators between baryon number and strangeness, which will be needed in the procedure described below, are defined as follows

$$\chi_{jk}^{BS}(T,\mu_B) = \left(\frac{\partial}{\partial \mu_B/T}\right)^j \left(\frac{\partial}{\partial \mu_S/T}\right)^k \frac{p(T,\mu_B)}{T^4} . \tag{63}$$

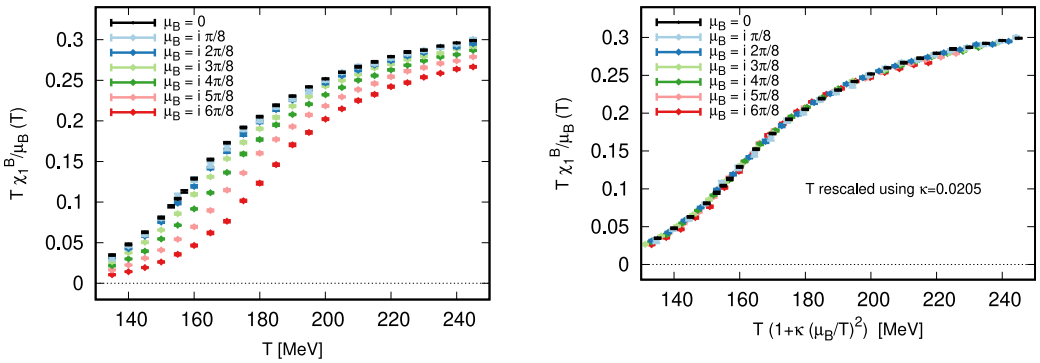


**Fig. 13.** From Ref. [19]. Left panel: The (imaginary) baryon density at simulated (imaginary) baryon chemical potentials, divided by the chemical potential. The points at $\mu_B = 0$ (black) show the second baryon susceptibility $\chi_2^B(T)$. Right panel: same curves as in the left panel, with a temperature rescaled in accordance to Eq. (65) with $\kappa = 0.0205$.

They have phenomenological relevance [149] and can also be used to extrapolate the equation of state of QCD in the full, four-dimensional phase diagram [146,147]. We will use the $\hat{\mu}_i = \mu_i/T$ shorthand notation in the following.

As discussed above, higher order derivatives of the pressure are notoriously difficult to calculate, because they suffer from a low signal-to-noise ratio due to large cancellations of different terms containing derivatives of the Dirac operator [150].

In Ref. [139], it was pointed out that the linear $\mu_B^2$-dependence of the crossover temperature may explain the basic structure of the higher order coefficients.

The complicated temperature-dependence of the higher order coefficients means that including one more term in a truncated Taylor series will not always improve the convergence. Pathological behavior such as non-monotonicity in the $T$- or $\mu_B$-dependence, can actually appear in the extrapolated thermodynamic quantities at chemical potentials beyond $\mu_B/T \sim 2{-}2.5$. This is due to the fact that, at large enough $\mu_B/T$, the observables at finite chemical potential are dominated by the $\mu_B = 0$ temperature dependence of the last coefficient included in the expansion. Therefore, the structures appearing in higher order coefficients around the QCD transition temperature are "translated" into the finite-$\mu_B$ behavior of e.g., the entropy, baryon density, etc.

An alternative summation scheme was presented in Ref. [19], which can better cope with the fact that the QCD transition temperature presents a $\mu_B$-dependence. The starting point is an observation based on Fig. 13. In the left panel of Fig. 13, temperature scans of the quantity $n_B(T)/\hat{\mu}_B = \chi_1^B(T, \hat{\mu}_B)/\hat{\mu}_B$ for several fixed imaginary $\mu_B/T$ ratios are shown. In the $\mu_B = 0$ limit, this quantity equals $\chi_2^B(T)$.

In the right panel of Fig. 13, all the finite-$\hat{\mu}_B$ curves have been shifted in accordance to the following equation

$$\frac{\chi_1^B(T, \hat{\mu}_B)}{\hat{\mu}_B} = \chi_2^B(T', 0) \,, \tag{64}$$

where the actual temperature difference can be expressed through a $\mu_B$-dependent rescaling factor that we write for simplicity as

$$T' = T\left(1 + \kappa \hat{\mu}_B^2\right) \,. \tag{65}$$

We note that the curves are very nicely superimposed to each other, even with the simple assumption of a single, $T$-independent parameter $\kappa = 0.0205$.

A similar behavior is observed for other quantities too, such as the first and second order fluctuations of strangeness, albeit with different $\kappa$ parameters.

*4.7.2. Formalism*

At $\mu_B = 0$, the normalized baryon density can be expressed as a Taylor expansion:

$$\frac{\chi_1^B}{\hat{\mu}_B}(T, \hat{\mu}_B) = \chi_2^B(T, 0) + \frac{\hat{\mu}_B^2}{6}\chi_4^B(T, 0) + \frac{\hat{\mu}_B^4}{120}\chi_6^B(T, 0) + \cdots \,. \tag{66}$$

Fig. 13 shows that the behavior of $\frac{\chi_1^B}{\hat{\mu}_B}(T, \hat{\mu}_B)$ at finite chemical potential closely resembles that of $\chi_2^B(T, \hat{\mu}_B)$, albeit shifted/rescaled in temperature. As long as $\chi_1^B/\hat{\mu}_B$ is a monotonic function of $T$, the $T'(T, \hat{\mu}_B)$ function can encode the finite density physics. A systematic generalization of Eq. (65) reads:

$$T'(T, \hat{\mu}_B) = T\left(1 + \kappa_2^{BB}(T)\hat{\mu}_B^2 + \kappa_4^{BB}(T)\hat{\mu}_B^4 + \mathcal{O}(\hat{\mu}_B^6)\right) \,. \tag{67}$$

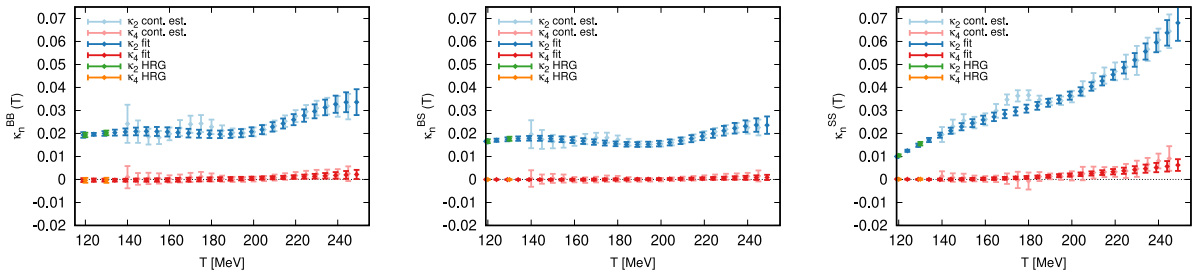


**Fig. 14.** From Ref. [19]. Results of the polynomial fits to $\kappa_2^{BB}$ and $\kappa_4^{BB}$ (left panel), $\kappa_2^{BS}(T)$ and $\kappa_4^{BS}(T)$ (central panel), and $\kappa_2^{SS}(T)$ and $\kappa_4^{SS}(T)$ (right panel). The parameters $\kappa_2^{ij}$ are shown in blue, and the $\kappa_4^{ij}$ in red. The fitted quantities are shown by lighter blue and red points. The HRG points are shown as green and orange dots.

In the above equation, we introduce the new parameters $\kappa_2^{BB}(T)$ and $\kappa_4^{BB}(T)$, which describe the shift/rescaling of the temperature of $\chi_1^B/\hat{\mu}_B$ at finite $\mu_B$. This formalism replaces the fixed temperature $\mu_B$ expansion by a fixed-observable (density) temperature expansion.

We now have two expressions, Eqs. (66) and (64), for the same quantity. We require them to be equal at each order in the $\hat{\mu}_B$ expansion at $\mu_B = 0$. We thus get:

$$\chi_4^B(T) = 6T\kappa_2^{BB}(T)\frac{d\chi_2}{dT} \ , \tag{68}$$
$$\chi_6^B(T) = 60T^2(\kappa_2^{BB})^2(T)\frac{d^2\chi_2}{dT^2} + 120T\kappa_4^{BB}(T)\frac{d\chi_2}{dT} \ ,$$

which in turn yields:

$$\kappa_2^{BB}(T) = \frac{1}{6T}\frac{\chi_4^B(T)}{\chi_2^{B'}(T)} \ , \tag{69}$$
$$\kappa_4^{BB}(T) = \frac{1}{360\chi_2^{B'}(T)^3}\left(3\chi_2^{B'}(T)^2\chi_6^B(T) - 5\chi_2^{B''}(T)\chi_4^B(T)^2\right) \ .$$

A similar treatment can be applied to the other observables.

*4.7.3. Lattice determination of the expansion coefficients*

The lattice action and the parameters used for this simulation are described in Ref. [150]. The gauge sector of the action benefits from tree-level Symanzik improvement, while quarks are treated in the staggered formalism with four levels of stout smearing. The up and down quarks are degenerate, and their mass is the physical one, as is the strange quark mass. Results are continuum extrapolated.

$\kappa_2^{BB}(T)$ was calculated using Eq. (69). To determine $\kappa_4^{BB}(T)$, imaginary chemical potential simulations were used as follows. Simulations at imaginary values of the baryon chemical potential:

$$\hat{\mu}_B = i\frac{n\pi}{8} \ , \qquad n \in \{3, 4, 5, 6\} \tag{70}$$

were performed, with $\hat{\mu}_Q = \hat{\mu}_S = 0$.

The simulated temperatures were in the range $T = 135$–$245$ MeV. For each temperature $T$ and chemical potential $\hat{\mu}_B$, the temperature $T'$ for which Eq. (66) holds was determined. This led to the definition of a function $T'(T, \hat{\mu}_B)$. Rearranging the terms in Eq (67), one can write:

$$\Pi(T, \hat{\mu}_B) = \kappa_2^{ij}(T') + \kappa_4^{ij}(T')\hat{\mu}_B^2 + \kappa_6^{ij}(T')\hat{\mu}_B^4 + \cdots \tag{71}$$

where the proxy quantity

$$\Pi(T, \hat{\mu}_B) = \frac{T'(T, \hat{\mu}_B) - T}{T'(T, \hat{\mu}_B)\hat{\mu}_B^2}. \tag{72}$$

was introduced. This proxy can be determined using lattice simulations. After determining $\Pi(T, \hat{\mu}_B)$ for several imaginary chemical potentials and several lattice spacings, and each given temperature, the expansion coefficients can be obtained by performing a polynomial fit in $\hat{\mu}_B^2$.

In the left panel of Fig. 14, the lighter points show the results of the temperature-by-temperature fit procedure for $\kappa_2^{BB}(T)$ and $\kappa_4^{BB}(T)$. The corresponding expectations from the HRG model are shown at low temperatures. It turns out that, within errors, $\kappa_2^{BB}(T)$ has hardly any dependence on the temperature, while $\kappa_4^{BB}(T)$ is everywhere consistent with zero at

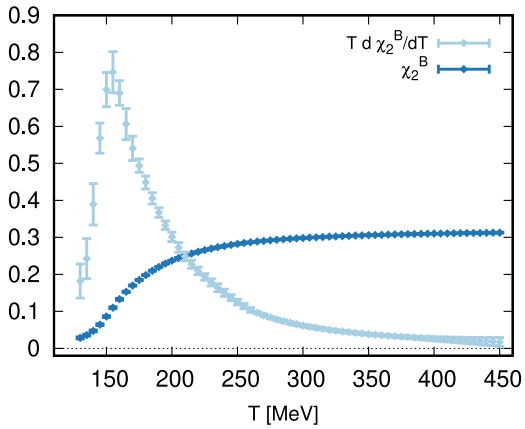


**Fig. 15.** From Ref. [19]. Continuum extrapolated $\chi_2^B(T)$ and $Td\chi_2^B(T)/dT$ functions from $N_\tau = 10$, 12 and 16 lattices at $\mu_B = 0$. Together with $\kappa_n^{BB}(T)$ these functions enter the thermodynamic analysis.

our current level of precision. The central and right panels of Fig. 14 show results for $\kappa_2^{BS}$, $\kappa_4^{BS}$ and $\kappa_2^{SS}$, $\kappa_4^{SS}$ respectively, together with their HRG prediction. A smoother version for the final results for $\kappa_2^{ij}$ and $\kappa_4^{ij}$ was constructed through a polynomial fit, in order to limit the influence of numerical effects on the final observables, but also to facilitate the temperature derivatives that enter the entropy formula. Fig. 14 shows the results of the fits in darker color.

A continuum result for the basic quantity $\chi_2^B(T, 0)$ is required, in addition to $\kappa_2^{BB}(T)$ and $\kappa_4^{BB}(T)$, in order to extract the thermodynamic quantities at finite chemical potential. For some observables, the temperature derivative of $\chi_2^B(T)$ is needed as well. The results for $Td\chi_2^B(T, 0)/dT$ and $\chi_2^B(T, 0)$ are shown in Fig. 15.

*4.7.4. Thermodynamics at real chemical potential*

Once $n_B$ is determined, the other thermodynamic quantities can be extracted making use of thermodynamic relationships. Dimensionless thermodynamic quantities, which correspond to the physical ones divided by suitable powers of the temperature, will be used. E.g., the dimensionful baryon density is $n_B = T^3\hat{n}_B$.

From the baryon density $\hat{n}_B(\hat{\mu}_B, T)$, the pressure is obtained through simple integration:

$$\frac{p(\mu_B, T)}{T^4} = \hat{p}(\hat{\mu}_B, T) = \hat{p}(0, T) + \int_0^{\hat{\mu}_B} \mathrm{d}\hat{\mu}'_B\, \hat{n}_B(\hat{\mu}'_B, T)\ . \tag{73}$$

The integration constant is taken as the pressure itself at $\mu_B = 0$.

The entropy density can be obtained as:

$$s(\mu_B, T) = \left.\frac{\partial p(\mu_B, T)}{\partial T}\right|_\mu . \tag{74}$$

For dimensionless quantities:

$$\hat{s}(\hat{\mu}_B, T) = 4\,\hat{p}(\hat{\mu}_B, T) + T\ \left.\frac{\partial \hat{p}(\hat{\mu}_B, T)}{\partial T}\right|_\mu = 4\,\hat{p}(\hat{\mu}_B, T) + T\ \left.\frac{\partial \hat{p}(\hat{\mu}_B, T)}{\partial T}\right|_{\hat{\mu}} - \hat{\mu}_B\hat{n}_B(\hat{\mu}_B, T). \tag{75}$$

In the last step, the derivative at constant $\mu_B$ was converted into a derivative at constant $\hat{\mu}_B$.

The $T$-derivative of the pressure involves the chain rule

$$T\ \left.\frac{\partial \hat{p}(\hat{\mu}_B, T)}{\partial T}\right|_{\hat{\mu}} = T\ \left.\frac{\partial \hat{p}(0, T)}{\partial T}\right|_{\hat{\mu}} + \frac{1}{2}\int_0^{\hat{\mu}_B^2} T\ \left.\frac{d\chi_2^B(T')}{dT'}\right|_{T'=T\left(1+\kappa_2^{BB}y+\kappa_4^{BB}y^2\right)} \times\left[1 + \kappa_2^{BB}y + \kappa_4^{BB}y^2 + T\left(\frac{d\kappa_2^{BB}}{dT}y + \frac{d\kappa_4^{BB}}{dT}y^2\right)\right] dy$$

where $\frac{d\chi_2^B(T)}{dT}$ has been calculated at $\mu_B = 0$ as described.

The dimensionless expression for the energy density $\hat{\epsilon} = \epsilon/T^4$ then follows:

$$\hat{\epsilon}(\hat{\mu}_B, T) = \hat{s}(\hat{\mu}_B, T) - \hat{p}(\hat{\mu}_B, T) + \hat{\mu}_B\hat{n}_B(\hat{\mu}_B, T). \tag{76}$$

The various panels of Fig. 16 show results for the baryon density, pressure, entropy, energy density, strangeness density and $\chi_2^S$ as functions of the temperature, for $\hat{\mu}_B = 0 - 3.5$. In all cases, it is evident that the observables do not suffer from

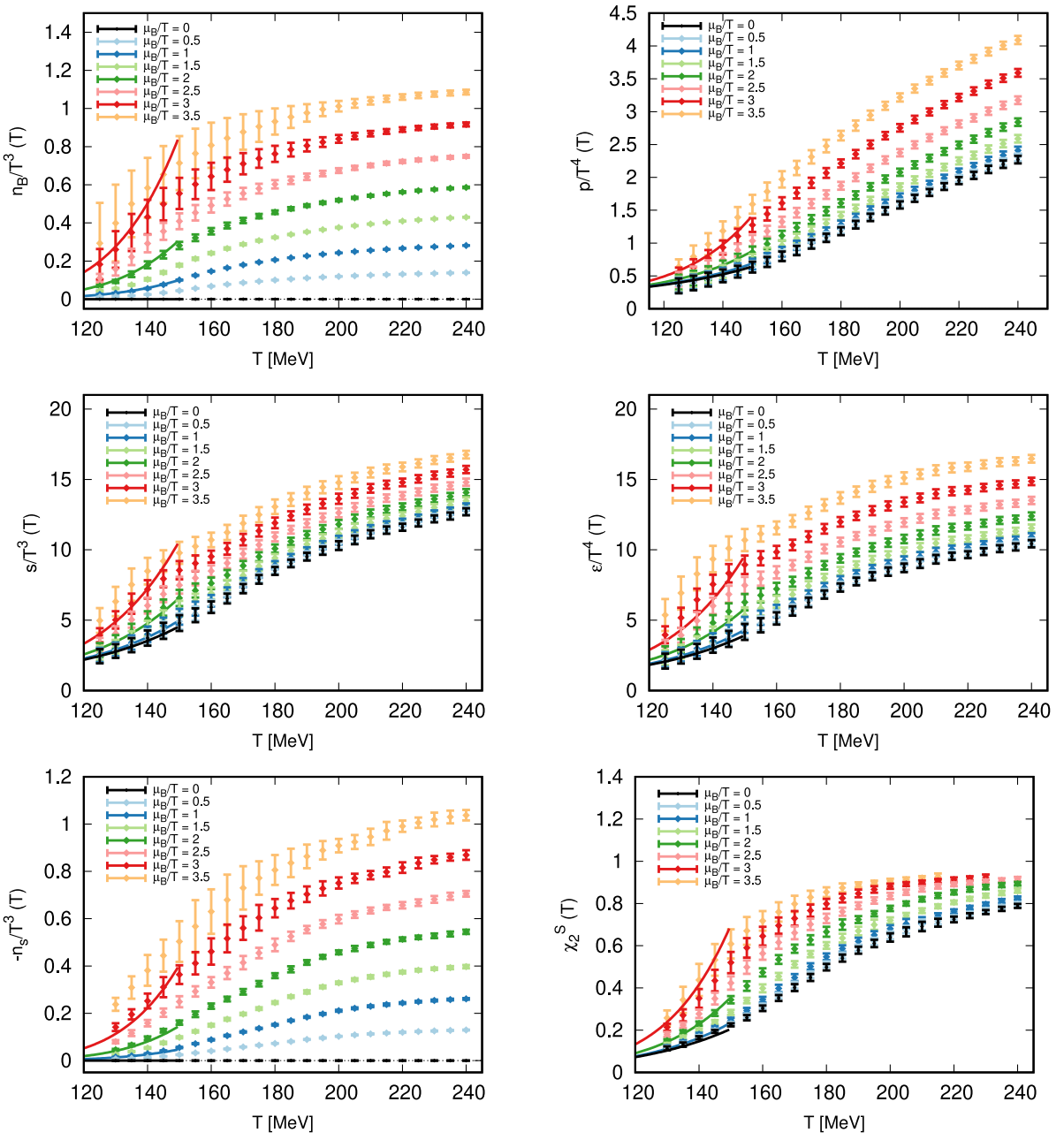


**Fig. 16.** From Ref. [19]. Baryon density, pressure, entropy, energy density, strangeness density and $\chi_2^S$ at different values of $\hat{\mu}_B$. The solid lines show the results from the HRG model.

pathological behavior. The two panels of Fig. 17 show the comparison of the baryon density (left) and energy density (right) to the case where $\kappa_4^{BB}$ is neglected. The inclusion of the next-to-leading-order parameter leads to an increased uncertainty at larger chemical potential, but does not change the value of the observable. This is an indication of the improved convergence properties of this expansion scheme, compared to the Taylor series. Recently, this equation of state was extended to the strangeness-neutral case, and even to finite strangeness, in Ref. [151].

To conclude this section it is important to point out that the method proposed in Ref. [19] is an expansion, which can be considered a resummation of the Taylor series. It is based on results obtained at zero and negative $\mu_B^2$, extrapolated to real values of $\mu_B$. For this reason, exactly like a Taylor series, it will break down in the vicinity of a critical point.

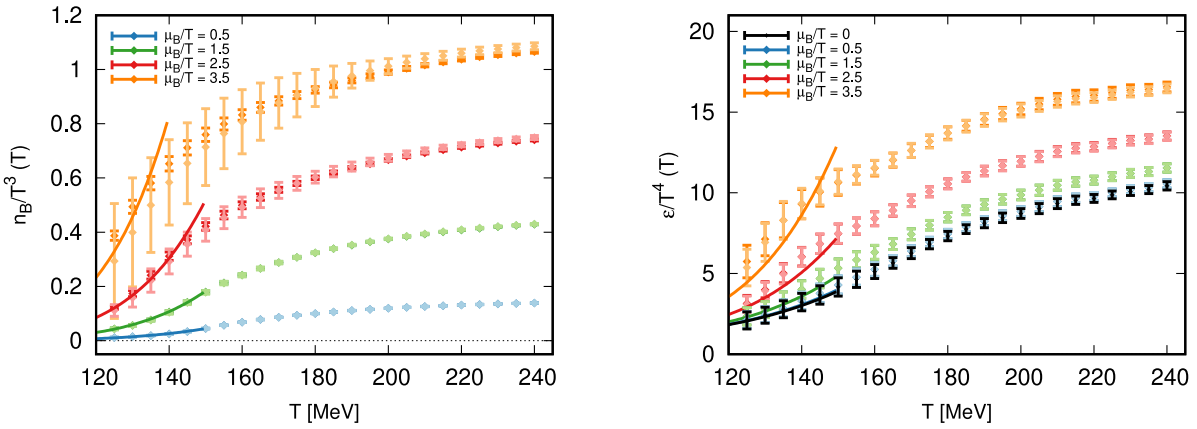


**Fig. 17.** From Ref. [19]. Comparison, for baryon density (left) and energy density (right) at different values of $\hat{\mu}_B$, between the case where a $\kappa_4^{BB}$ parameter is used (darker shades) or omitted (lighter shades). The solid lines at low temperature are the HRG model results.

### *4.8. Other observables at finite chemical potential*

While this review is about the equation of state of QCD, it is worth mentioning that significant progress has been achieved in lattice QCD simulations of other fundamental quantities at finite density. The transition line of QCD, namely the change of the transition temperature with the baryonic chemical potential, has been thoroughly studied by several groups [152–171], including constraints on the location of the critical point. Fluctuations of conserved charges have also been investigated [172–177]. They are typically either compared to experimental observables in order to extract the chemical freeze-out parameters as a function of the collision energy [178–186], or they are used to constrain the spectrum and the interaction to be included in the HRG [187–203] or other phenomenological models.

## 5. Other approaches at high chemical potential

Several alternative methods have been developed in the literature, in order to expand the above results to larger chemical potential or to study the critical point effects explicitly. I will briefly review a few recent ones here, focusing on the ones that calculated the equation of state of QCD at large $\mu_B$.

### *5.1. Dyson–Schwinger equation*

Dyson–Schwinger equations (DSE) and the functional renormalization group (FRG) provide an alternative approach to study QCD at finite density. However, this approach typically relies on approximations that are less controlled than the lattice QCD ones. A way of controlling these approximations is by imposing constraints derived from symmetries, and by reproducing lattice QCD results when available. In this approach, the gluon degrees of freedom, which are usually integrated out in the other effective models such as Nambu Jona-Lasinio, Polyakov-loop-extended Nambu Jona-Lasinio or Quark Meson model, are instead directly accessible. For a recent review of Dyson–Schwinger results see Ref. [204].

Several results for QCD thermodynamics and susceptibilities are available from different groups, using different truncation schemes. For example, the authors of Ref. [205] calculated the normalized pressure and trace anomaly both at zero and finite quark chemical potential. In Ref. [206], the thermodynamics of QCD has been studied at chemical potentials larger than the critical point one, to study the behavior in the presence of a first order phase transition. Quark number susceptibilities have been studied in Ref. [207]. More recently, the authors of Ref. [208] presented a method to compute thermodynamic quantities, within functional continuum frameworks, that is independent of the employed truncation. Fig. 18 shows the scaled entropy density, pressure and energy density obtained in this method.

FRG approaches have been used to enhance more phenomenological models beyond mean field. Several thermodynamic quantities have been explored in this case see e.g. Refs. [209–214].

### *5.2. Equation of state in the black hole engineering approach*

Among the approaches to extend QCD to higher baryon densities, black hole engineering [215,216] has been very successful. It is based on the holographic correspondence [217], a well-known tool developed in string theory, and it is the only model that fulfills the following conditions: it reproduces the thermodynamics of QCD in the crossover region at zero and small baryon density, and the perfect fluidity behavior observed in heavy-ion collisions.

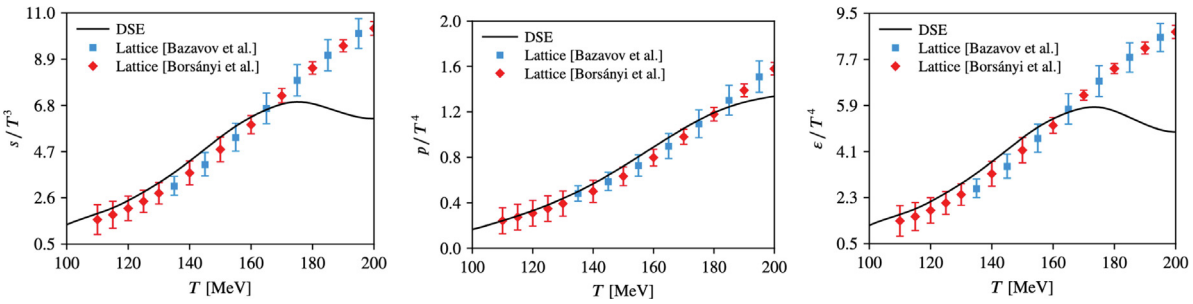


**Fig. 18.** From Ref. [208]. Scaled entropy density (left), pressure (center) and energy density (right) obtained from a Dyson–Schwinger approach. The lattice results are from Refs. [48,50].

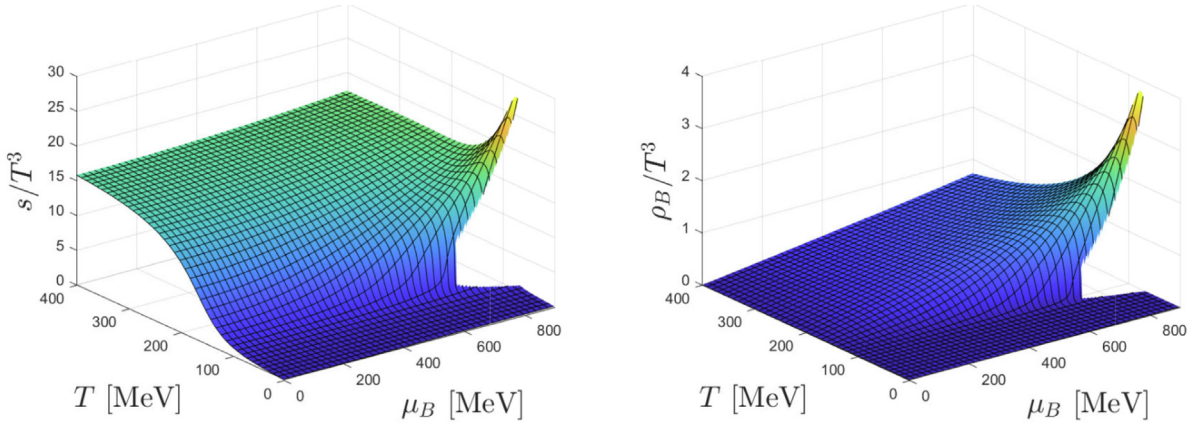


**Fig. 19.** From Ref. [246]. Left: scaled entropy in the $(T, \mu_B)$ plane determined from black hole engineering. Right: scaled baryonic density in the $(T, \mu_B)$ plane.

In Ref. [218], a realistic black hole engineering model was constructed, and it was shown to reproduce the QCD thermodynamic Taylor coefficients displayed in Section 4.5 up to $\chi_8^B$. This construction mainly differs from the earlier developments of [215,219,220] by the fact that old lattice data were used in those previous holographic works to fix the free parameters of the model. Some previous holographic approaches focusing on qualitative aspects of the strongly coupled QGP can be seen e.g. in Refs. [221–245].

Ref. [218] makes use of state-of-the-art lattice QCD results at $\mu_B = 0$ as first principles inputs from QCD to fix the free parameters of the EMD model. In this configuration, the model predicts the existence of a critical point on the QCD phase diagram at $T = 89$ MeV and $\mu_B = 724$ MeV, corresponding to a collision energy $\sqrt{s} = 2.5 - 4.1$ GeV. The equation of state of the model, for a large coverage of temperature and chemical potential, has been obtained in Ref. [246]. Entropy and baryon density as functions of temperature and chemical potential are shown in Fig. 19.

### 5.3. Lattice-based approach with a 3D-Ising model critical point

The QCD critical point, if it exists, should be in the 3D-Ising model universality class [163,247–250]. Ref. [251] made use of this information to construct a family of Equations of State for QCD, which match results from lattice simulations up to order $\mu_B^4$, and exhibit the correct scaling behavior in the vicinity of the critical point. This approach contains four free parameters, including the location of the critical point and the strength of the critical region, that can be chosen by the user to test the critical point effect.

The construction of this family of equations of state follows the procedure detailed below:

- a non-universal mapping is postulated, between the Ising model phase diagram in the variables $r = (T - T_c)/T_c$ (reduced temperature) and $h$ (magnetic field), and the QCD phase diagram in the variables $T$ and $\mu_B$

$$\begin{aligned} \frac{T - T_C}{T_C} &= w(r\rho \sin\alpha_1 + h \sin\alpha_2) \\ \frac{\mu_B - \mu_{BC}}{T_C} &= w(-r\rho \cos\alpha_1 - h \cos\alpha_2), \end{aligned} \tag{77}$$

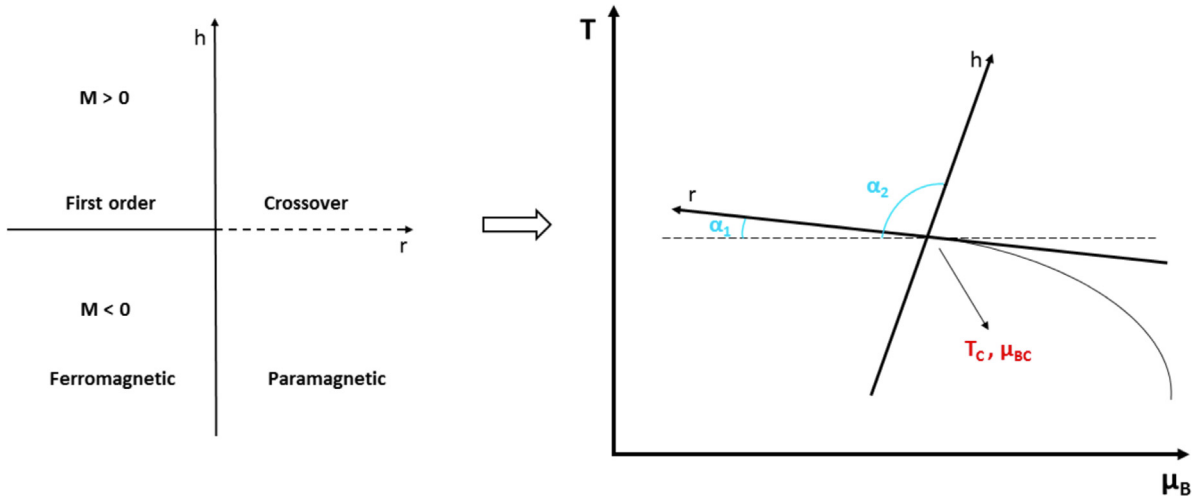


**Fig. 20.** From Ref. [251]. Map from Ising variables $(r, h)$ to QCD coordinates $(T, \mu_B)$ used in this approach.

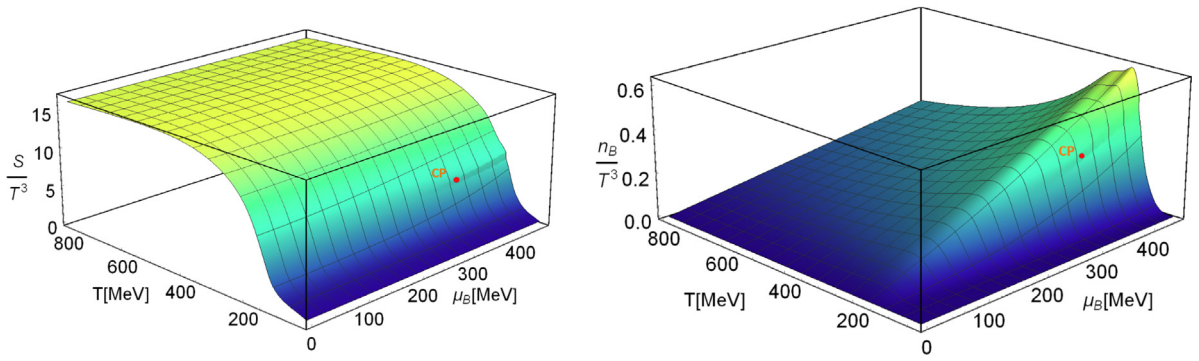


**Fig. 21.** From Ref. [251]. Entropy density (left) and baryonic density (right) as functions of the temperature and chemical potential. The red dot marks the position of the critical point. Both quantities exhibit a discontinuity for $\mu_B > \mu_{BC}$, as expected.

where $T_C$ and $\mu_{BC}$ are the temperature and chemical potential of the critical point, $\alpha_1$ and $\alpha_2$ are the angles that the $r$ and $h$ axes form with the $T$ =const. lines, and $(w, \rho)$ are scale factors for the variables $r$ and $h$ (see Fig. 20);

- the assumption is made, that the lattice QCD Taylor expansion coefficients discussed in Section 4.5 receive an "Ising" contribution coming from the critical point of QCD, and a non-Ising contribution, which contains the regular part as well as any other possible criticality present in the region of interest, but not related to the critical point:

$$T^4 c_n^{LAT}(T) = T^4 c_n^{Non-Ising}(T) + T_C^4 c_n^{Ising}(T). \tag{78}$$

Thus, the family of Equations of State extracted with this prescription reproduces the lattice QCD results for the pressure and its Taylor coefficients up to the desired order by construction. The full pressure is then reconstructed as

$$P(T, \mu_B) = T^4 \sum_n c_{2n}^{Non-Ising}(T) \left(\frac{\mu_B}{T}\right)^{2n} + P_{crit}^{QCD}(T, \mu_B). \tag{79}$$

The entropy density (left) and the baryonic density (right), obtained in this approach for one specific parameter choice, are shown in Fig. 21. For a version of this equation of state that matches the phenomenological conditions of strangeness neutrality and electric charge conservation, see Ref. [252].

## 6. QCD at finite isospin chemical potential

Numerical simulations of QCD at finite isospin chemical potential are not affected by the sign problem and can therefore be performed using Monte Carlo techniques. The fermionic part of the Euclidean QCD Lagrangian is modified as follows

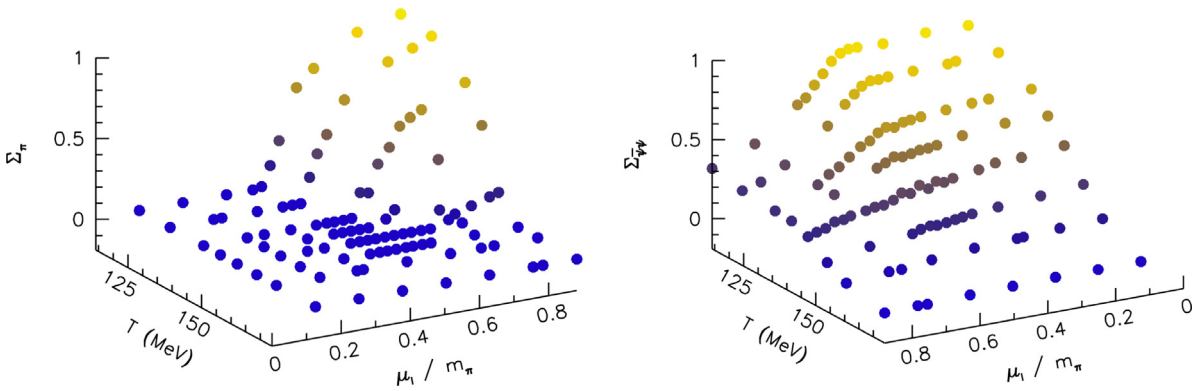


**Fig. 22.** From Ref. [253]. Pion condensate (left) and quark condensate (right) as functions of temperature and isospin chemical potential.

when we introduce a finite $\mu_I$:

$$\begin{aligned} S_{ud} &= \bar{\psi} M_{ud} \psi \\ M_{ud} &= \gamma^\mu(\partial_\mu + iG_\mu)\mathbb{1} + m_{ud}\mathbb{1} + \mu_I \gamma_4 \tau_3 + i\lambda\gamma_5\tau_2, \end{aligned} \tag{80}$$

where $G_\mu$ is the gluon field and $\tau_a$ the Pauli matrices. The term proportional to $\lambda$ is needed in a finite volume to trigger the spontaneous breaking of the $U_{\tau_3}(1)$ symmetry due to the chemical potential. This is an explicit symmetry breaking term that couples to the charged pion field. Results are then extrapolated to $\lambda \to 0$.

The lattice QCD partition function can be written as

$$Z = \int [DU] e^{-\beta S_G} (\det M_{ud})^{1/4} (\det M_s)^{1/4}, \tag{81}$$

where

$$M_{ud} = \begin{pmatrix} \not{D}(\mu_I) + m_{ud} & \lambda\eta_5 \\ -\lambda\eta_5 & \not{D}(-\mu_I) + m_{ud} \end{pmatrix} \tag{82}$$

where $\eta_5 = (-1)^{m_x+m_y+m_z+m_t}$ and the $m_i$ are the lattice site coordinates. It is evident that the isospin chemical potential is introduced on the lattice by multiplying the forward and backward timelike links by $e^{a\mu_I}$ and $e^{-a\mu_I}$, respectively.

The staggered fermion equivalent of chiral symmetry implies that

$$\not{D}(\mu_I)\eta_5 + \eta_5 \not{D}(\mu_I) = 0 \tag{83}$$

holds. The following condition is satisfied by the Dirac operator

$$\eta_5 \not{D}(\mu_I)\eta_5 = \not{D}(\mu_I)^\dagger. \tag{84}$$

Therefore, the light fermion determinant obeys

$$\tau_1 \eta_5 M_{ud} \eta_5 \tau_1 = M_{ud}^\dagger. \tag{85}$$

Taking the determinant of both sides shows that $\det(M_{ud})$ is real. It is also positive, because if we consider

$$M'_{ud} = B M_{ud} B = \begin{pmatrix} \not{D}(\mu_I) + m_{ud} & \lambda \\ -\lambda & [\not{D}(\mu_I) + m_{ud}]^\dagger \end{pmatrix} \tag{86}$$

where $B = \text{diag}(1, \eta_5)$, since $\det B = 1$ we get

$$\det M_{ud} = \det[(\not{D}(\mu_I) + m_{ud})\,(\not{D}(\mu_I) + m_{ud})^\dagger + \lambda^2] > 0. \tag{87}$$

Therefore, lattice QCD simulations based on importance sampling techniques can be performed at finite isospin chemical potential. Several results have been obtained in the literature. In Ref. [253], a system of $N_f = 2+1$ on $24^3 \times 6$ lattices has been considered, and the chiral condensate and the pion condensate have been simulated as functions of temperature and $\mu_I$. The two panels of Fig. 22 show the corresponding results.

The left panel of Fig. 23 shows the corresponding phase diagram. A triple point is found at $(T_C, \mu_{IC}) = (151(7), 70(5))$ MeV. This is consistent with expectations from the NJL model [254–258].

The right panel of Fig. 23 shows the contours of constant renormalized Polyakov loop. Since this observable does not show a pronounced inflection point as a function of the temperature, these curves capture the dependence of deconfinement on the isospin chemical potential: e.g. the contour for which the Polyakov loop is 1 can be chosen to

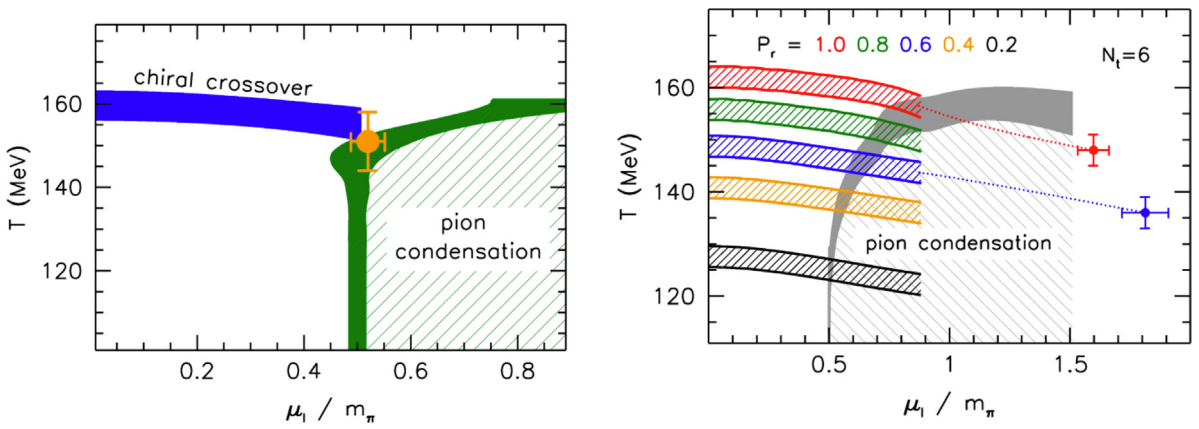


**Fig. 23.** From Ref. [253]. Left: phase diagram of QCD in the $(T, \mu_I)$ plane. The blue band is the chiral crossover transition temperature, while the green line is the boundary of the pion condensation phase. The triple point is marked by a yellow dot. Right: the colored bands indicate contour lines of constant renormalized Polyakov loop.

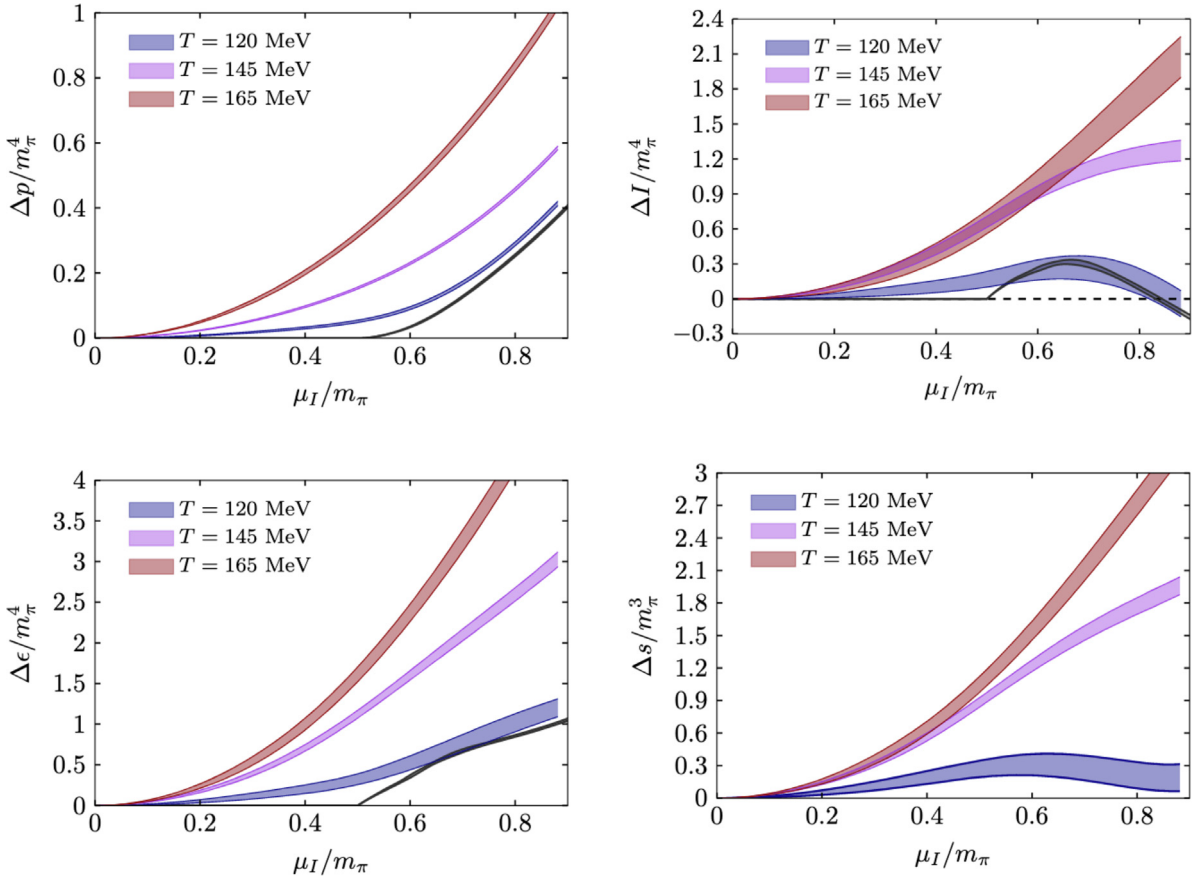


**Fig. 24.** From Ref. [259]. Thermodynamic quantities as functions of the isospin chemical potentials for different values of the temperature. The dark gray band corresponds to $T = 0$ (from Ref. [260]).

identify a transition temperature for deconfinement. It is interesting to notice that, contrary to the chiral phase transition line shown in the left panel of Fig. 23, these contour lines are insensitive to the pion condensation phase.

The equation of state of QCD at finite isospin chemical potential has been studied in Ref. [259]. Results for several quantities as functions of the isospin chemical potential are shown in Fig. 24 at different temperature values. The $T = 0$ curve shows the characteristic features of a first-order phase transition at $\mu_I/m_\pi = 0.5$.

## 7. Conclusions

In this manuscript I reviewed the state of the art of the QCD equation of state from lattice simulations at zero and finite chemical potential. The traditional Taylor expansion and imaginary chemical potential simulation methods have been described, with their limitations in the range of applicability in $\mu_B/T$. I also described a novel expansion scheme, which allows to almost double the coverage in chemical potential, and which shows improved convergence properties. The last part of this review is devoted to a few alternative methods, which are used to extend the lattice QCD results to the regions of the phase diagram that lattice simulations cannot cover yet. Continuous progress in the study of the equation of state has led to high precision results that can be used in phenomenological applications.

The equation of state is a crucial set of observables to describe many physical phenomena. For example, it is used as input in hydrodynamic simulations of heavy-ion collisions. With the advent of the second beam energy scan data from RHIC, it is crucial to have an equation of state that covers the whole range of $T$ and $\mu_B$ covered in experiments, and that allows phenomenologists to investigate the effect of a critical point/first order phase transition on actual data. The equations of state from first principles presented here need to be extended to larger chemical potentials. The same is true for the EoS with Ising model critical point, which right now is limited in its $\mu_B$ range by the lattice Taylor expansion. A combination of Ising model properties and new expansion schemes might allow us to push the study of critical effect to larger chemical potentials. Direct simulations at finite real $\mu_B$ are also starting to appear on coarse lattices [261]. These results are very promising: a realistic equation of state might become available soon.

The advent of gravitational wave signals from neutron star mergers opens up new exciting possibilities to constrain the equation of state at large densities. The shape of the gravitational wave signal is sensitive to the degrees of freedom in the core of neutron stars. In particular, a first-order phase transition to quark matter leaves a different imprint, compared to a smooth crossover. The next generation of gravitational wave observatories might have enough resolution to distinguish between the two.

## Acknowledgments

This material is based upon work supported by the National Science Foundation, USA under grants no. PHY-2208724,PHY-1654219 and PHY-2116686. This work was supported in part by the National Science Foundation (NSF) within the framework of the MUSES collaboration, under grant number OAC-2103680. C.R. also acknowledges the support from the Center of Advanced Computing and Data Systems at the University of Houston, USA.

## Appendix

The differential method was first proposed in Ref. [262]. Soon afterwards, it was noticed in Ref. [263] that it can lead to a negative pressure near the critical temperature. Ref. [264] presented a proposal to improve the method. For more details see [265]. Both derivatives with respect to $T$ and $V$ are needed to calculate the thermodynamic quantities. In order to distinguish between them, the theory is defined on a $(3+1)$-dimensional anisotropic lattice, having different lattice spacings in the spatial ($a_s$) and temporal ($a_t$) directions. One then usually replaces the variables $\{T, V\}$ by the anisotropy parameter $\xi$ and a scale $a$, as follows

$$\xi = \frac{a_s}{a_t}, \qquad a = a_s. \tag{88}$$

One can then re-express the partial derivatives with respect to $T$ and $V$ in terms of the new variables $\xi$ and $a$, at fixed $N_s$ and $N_t$:

$$T\,\frac{\partial}{\partial T}\bigg|_V = \xi\,\frac{\partial}{\partial \xi}\bigg|_a \qquad \text{and} \qquad 3V\,\frac{\partial}{\partial V}\bigg|_T = a\,\frac{\partial}{\partial a}\bigg|_\xi + \xi\,\frac{\partial}{\partial \xi}\bigg|_a . \tag{89}$$

The pure gauge action in an isotropic, four-dimensional hypercube can be written as

$$S_G = \sum_{x\mu\nu} \frac{1}{g^2 a^4} tr\left\{1 - \Re U_{\mu\nu,x}\right\}. \tag{90}$$

In the above equation and in the rest of the manuscript, the symbol $\Re$ indicates "the real part". Now we need to modify this expression, to take into account the two different lattice spacings in the spatial and temporal directions. In the equation above, we have

$$U_{\mu\nu,x} = U^\dagger_{\nu\mu,x} = U_{x,x+a\hat{\mu}} U_{x+a\hat{\mu},x+a\hat{\mu}+a\hat{\nu}} U_{x+a\hat{\mu}+a\hat{\nu},x+a\hat{\nu}} U_{x+a\hat{\nu},x}. \tag{91}$$

We define $P_{\mu\nu}(x) = 1 - \frac{\Re tr U_{\mu\nu,x}}{N_c}$, and we introduce the following notation for the average spatial and temporal plaquettes

$$P_s = \sum_{x,j>i,i,j=1}^{3} \frac{P_{ij}(x)}{3N_s^3 N_t}, \qquad P_t = \sum_{x,i=1}^{3} \frac{P_{0i}(x)}{3N_s^3 N_t}. \tag{92}$$

The Wilson action in this case can be written as

$$S_G[U] = 6N_c N_s^3 N_t \left[\kappa_s P_s + \kappa_t P_t\right] \tag{93}$$

with

$$\kappa_s = \frac{1}{\xi g_s^2} \qquad \text{and} \qquad \kappa_t = \frac{\xi}{g_t^2} \tag{94}$$

where $g_s$ and $g_t$ are the gauge couplings along the spatial and temporal directions, respectively. Using these definitions, we obtain

$$\epsilon = \frac{T^2}{V}\frac{\partial \ln Z}{\partial T} = \frac{T}{V}\xi\frac{\partial \ln Z}{\partial \xi} = -\frac{T}{V}\frac{\xi \int DU \frac{\partial S_G[U]}{\partial \xi} e^{-S_G[U]}}{Z}. \tag{95}$$

We can then re-write

$$\begin{aligned}\epsilon &= \frac{\xi^2}{N_t N_s^3 a^4}\frac{\int DU \left(-\frac{\partial S_G[U]}{\partial \xi}\right) e^{-S_G[U]}}{Z} = -\frac{\xi^2 6N_c N_s^3 N_t}{N_s^3 N_t a^4}\left[\frac{\partial \kappa_s}{\partial \xi}\langle P_s\rangle + \frac{\partial \kappa_t}{\partial \xi}\langle P_t\rangle\right] \\ &= -\frac{\xi^2 6N_c}{a^4}\left[\frac{\partial \kappa_s}{\partial \xi}\langle P_s\rangle + \frac{\partial \kappa_t}{\partial \xi}\langle P_t\rangle\right],\end{aligned} \tag{96}$$

where we used the following identity

$$\frac{\partial S_G[U]}{\partial \xi} = \left[\frac{\partial \kappa_s}{\partial \xi}P_s + \frac{\partial \kappa_t}{\partial \xi}P_t\right] 6N_c N_s^3 N_t, \tag{97}$$

and the fact that

$$T = \frac{\xi}{N_t a}, \qquad V = N_s^3 a^3. \tag{98}$$

The energy density above contains a vacuum contribution that can be eliminated by subtracting $\epsilon(T=0)$. This contribution is similar to the zero-point energy of the continuum theory. We can approximate it by calculating $\epsilon$ on the symmetric $N_s^4$ lattice at sufficiently large $N_s$; we thus get

$$a^4\epsilon = -6N_c\xi^2\left[\frac{\partial \kappa_s}{\xi}D_s + \frac{\partial \kappa_t}{\partial \xi}D_t\right] \tag{99}$$

where $D_i = \langle P_i\rangle - \langle P_0\rangle$ and $\langle P_0\rangle$ is the average plaquette at $T=0$.

Analogously, we have

$$\begin{aligned}p &= T\frac{\partial \ln Z}{\partial V} = \frac{T}{3V}\left[a\frac{\partial \ln Z}{\partial a} + \xi\frac{\partial \ln Z}{\partial \xi}\right] \\ &= -\frac{\frac{T}{3V}a\left[\int DU \frac{\partial S_G[U]}{\partial a} e^{-S_G[U]}\right]}{Z} - \frac{\frac{T}{3V}\xi\left[\int DU \frac{\partial S_G[U]}{\partial \xi} e^{-S_G[U]}\right]}{Z}.\end{aligned} \tag{100}$$

We now use the identities

$$\begin{aligned}\frac{\partial S_G[U]}{\partial a} &= 6N_c N_s^3 N_t\left[\frac{\partial \kappa_s}{\partial a}P_s + \frac{\partial \kappa_t}{\partial a}P_t\right] \\ \frac{\partial S_G[U]}{\partial \xi} &= 6N_c N_s^3 N_t\left[\frac{\partial \kappa_s}{\partial \xi}P_s + \frac{\partial \kappa_t}{\partial \xi}P_t\right].\end{aligned} \tag{101}$$

and subtracting the zero-point pressure we get

$$a^4 p = -2N_c\xi^2\left[\frac{\partial \kappa_s}{\partial \xi}D_s + \frac{\partial \kappa_t}{\partial \xi}D_t\right] - 2N_c\xi a\left[\frac{\partial \kappa_s}{\partial a}D_s + \frac{\partial \kappa_t}{\partial a}D_t\right]. \tag{102}$$

We also calculate the quantity $I = \epsilon - 3p$, the so-called interaction measure or "trace anomaly". This name follows from the fact that it is generated by the breaking of the conformal invariance of QCD at the quantum level. For the trace anomaly we get

$$a^4\Delta I = 6N_c\xi a\left[\frac{\partial \kappa_s}{\partial a}D_s + \frac{\partial \kappa_t}{\partial a}D_t\right]. \tag{103}$$

These expressions involve derivatives of the couplings $g_s$ and $g_t$ with respect to $a$ and $\xi$. We can expand the two $g_i^{-2}$ around their symmetric lattice value $g^{-2}(a)$ in the weak coupling limit [266] ($\xi = 1$ in the following)

$$g_i^{-2}(a,\xi) = g^2(a) + c_i(\xi) + \mathcal{O}(g^2(a)) \tag{104}$$

with the condition $c_i(\xi = 1) = 0$. We thus need to know

$$b(a) = a\frac{\partial g^{-2}(a)}{\partial a}. \tag{105}$$

Using the definition of the $\beta-$function calculated in perturbative QCD at one loop,

$$B(\alpha_s) = \frac{\mu}{2}\frac{\partial \alpha_s}{\partial \mu} = -\frac{33-2N_f}{12\pi}\alpha_s^2 + \cdots \qquad \alpha_s = \frac{g^2}{4\pi} \tag{106}$$

we get $b(a) = \frac{B(\alpha_s)}{2\pi\alpha_s^2}$ because

$$2B(\alpha_s) = a\frac{\partial \alpha_s}{\partial a} = a\frac{\partial \alpha_s}{\partial g^{-2}}\frac{\partial g^{-2}}{\partial a} \tag{107}$$

from which we get

$$\begin{aligned} a\frac{\partial \kappa_s}{\partial a} &= \frac{a}{\xi}\frac{\partial g_s^{-2}}{\partial a} = \frac{B}{2\pi\alpha_s^2\xi} \\ \frac{\partial \kappa_s}{\partial \xi} &= -\frac{g_s^{-2}}{\xi^2} + \frac{1}{\xi}\frac{\partial c_s}{\partial \xi} \\ a\frac{\partial \kappa_t}{\partial a} &= a\xi\frac{\partial g_t^{-2}}{\partial a} = \frac{\xi B}{2\pi\alpha_s^2} \\ \frac{\partial \kappa_t}{\partial \xi} &= -g_t^{-2} + \xi\frac{\partial c_t}{\partial \xi}. \end{aligned} \tag{108}$$

Putting everything together, in the $\xi \to 1$ limit we find

$$\begin{aligned} \frac{\epsilon}{T^4} &= 2\frac{N_c N_t^3}{N_s^3}\left[\frac{D_s - D_t}{g^2} - \left(\frac{\partial c_s}{\partial \xi}D_s + \frac{\partial c_t}{\partial \xi}D_t\right)\right] \\ \frac{p}{T^4} &= \frac{2}{3}\frac{N_c N_t^3}{N_s^3}\left[\frac{D_s - D_t}{g^2} - \left(\frac{\partial c_s}{\partial \xi}D_s + \frac{\partial c_t}{\partial \xi}D_t\right)\right] - \frac{2}{3}\frac{N_c N_t^3}{N_s^3}\frac{B}{2\pi\alpha_s^2}\left[D_s + D_t\right] \\ \frac{\Delta I}{T^4} &= 2\frac{N_c N_t^3}{N_s^3}\frac{B}{2\pi\alpha_s^2}\left[D_s + D_t\right]. \end{aligned} \tag{109}$$

It was suggested in the literature, that the fact that the pressure turns negative near the transition temperature is due to the use of perturbative formulas for the derivatives of the coupling. To cure this problem, the integral method was introduced in Refs. [267–269].

## References


[1] K. Adcox, et al., PHENIX, Nuclear Phys. A 757 (2005) 184–283, http://dx.doi.org/10.1016/j.nuclphysa.2005.03.086.
[2] I. Arsene, et al., BRAHMS, Nuclear Phys. A 757 (2005) 1–27, http://dx.doi.org/10.1016/j.nuclphysa.2005.02.130.
[3] B.B. Back, et al., PHOBOS, Nuclear Phys. A 757 (2005) 28–101, http://dx.doi.org/10.1016/j.nuclphysa.2005.03.084.
[4] J. Adams, et al., [STAR], Nuclear Phys. A 757 (2005) 102–183, http://dx.doi.org/10.1016/j.nuclphysa.2005.03.085, arXiv:nucl-ex/0501009 [nucl-ex].
[5] K. Aamodt, et al., [ALICE], J. Instrum. 3 (2008) S08002, http://dx.doi.org/10.1088/1748-0221/3/08/S08002.
[6] G. Aad, et al., ATLAS, J. High Energy Phys. 11 (2013) 183, http://dx.doi.org/10.1007/JHEP11(2013)183.
[7] S. Chatrchyan, et al., CMS, Phys. Rev. C 84 (2011) 024906, http://dx.doi.org/10.1103/PhysRevC.84.024906.
[8] Y. Aoki, G. Endrodi, Z. Fodor, S.D. Katz, K.K. Szabo, Nature 443 (2006) 675–678, http://dx.doi.org/10.1038/nature05120, arXiv:hep-lat/0611014 [hep-lat].
[9] M.A. Stephanov, Proc. Sci. LAT2006 (2006) 024, http://dx.doi.org/10.22323/1.032.0024, arXiv:hep-lat/0701002 [hep-lat].
[10] M. Nahrgang, Nuclear Phys. A 956 (2016) 83–90, http://dx.doi.org/10.1016/j.nuclphysa.2016.02.074, arXiv:1601.07437 [nucl-th].
[11] C. Ratti, Rep. Progr. Phys. 81 (8) (2018) 084301, http://dx.doi.org/10.1088/1361-6633/aabb97, arXiv:1804.07810 [hep-lat].
[12] A. Bzdak, S. Esumi, V. Koch, J. Liao, M. Stephanov, N. Xu, Phys. Rep. 853 (2020) 1–87, http://dx.doi.org/10.1016/j.physrep.2020.01.005, arXiv:1906.00936 [nucl-th].
[13] M.A. Stephanov, K. Rajagopal, E.V. Shuryak, Phys. Rev. Lett. 81 (1998) 4816–4819, http://dx.doi.org/10.1103/PhysRevLett.81.4816, arXiv:hep-ph/9806219 [hep-ph].
[14] D. Cebra, S.G. Brovko, C.E. Flores, B.A. Haag, J.L. Klay, arXiv:1408.1369 [nucl-ex].
[15] T. Galatyuk, HADES, Nuclear Phys. A 931 (2014) 41–51, http://dx.doi.org/10.1016/j.nuclphysa.2014.10.044.
[16] J. Adamczewski-Musch, et al., HADES, Nat. Phys. 15 (10) (2019) 1040–1045, http://dx.doi.org/10.1038/s41567-019-0583-8.
[17] E.R. Most, L.J. Papenfort, V. Dexheimer, M. Hanauske, S. Schramm, H. Stöcker, L. Rezzolla, Phys. Rev. Lett. 122 (6) (2019) 061101, http://dx.doi.org/10.1103/PhysRevLett.122.061101, arXiv:1807.03684 [astro-ph.HE].
[18] V. Dexheimer, J. Noronha, J. Noronha-Hostler, C. Ratti, N. Yunes, J. Phys. G 48 (7) (2021) 073001, http://dx.doi.org/10.1088/1361-6471/abe104, arXiv:2010.08834 [nucl-th].
[19] S. Borsányi, Z. Fodor, J.N. Guenther, R. Kara, S.D. Katz, P. Parotto, A. Pásztor, C. Ratti, K.K. Szabó, Phys. Rev. Lett. 126 (23) (2021) 232001, http://dx.doi.org/10.1103/PhysRevLett.126.232001, arXiv:2102.06660 [hep-lat].

[20] S. Borsanyi, G. Endrodi, Z. Fodor, S.D. Katz, K.K. Szabo, J. High Energy Phys. 1207 (2012) 056.
[21] S. Borsanyi, G. Endrodi, Z. Fodor, A. Jakovac, S.D. Katz, S. Krieg, C. Ratti, K.K. Szabo, J. High Energy Phys. 1011 (2010) 077.
[22] E.V. Shuryak, Sov. Phys.—JETP 47 (1978) 212; Zh. Eksp. Teor. Fiz. 74 (1978) 408.
[23] J.I. Kapusta, Nuclear Phys. B 148 (1979) 461.
[24] T. Toimela, Internat. J. Theoret. Phys. 24 (1985) 901, Erratum:; Int. J. Theor. Phys. 26 (1987) 1021.
[25] P.B. Arnold, C.x. Zhai, Phys. Rev. D 51 (1995) 1906.
[26] E. Braaten, A. Nieto, Phys. Rev. Lett. 76 (1996) 1417.
[27] E. Braaten, A. Nieto, Phys. Rev. D 53 (1996) 3421.
[28] C.x. Zhai, B.M. Kastening, Phys. Rev. D 52 (1995) 7232.
[29] K. Kajantie, M. Laine, K. Rummukainen, Y. Schroder, Phys. Rev. D 67 (2003) 105008.
[30] E. Braaten, R.D. Pisarski, Phys. Rev. D 45 (6) (1992) R1827.
[31] J.O. Andersen, E. Braaten, E. Petitgirard, M. Strickland, Phys. Rev. D 66 (2002) 085016.
[32] J.O. Andersen, E. Petitgirard, M. Strickland, Phys. Rev. D 70 (2004) 045001.
[33] J.O. Andersen, M. Strickland, N. Su, Phys. Rev. Lett. 104 (2010) 122003.
[34] J.O. Andersen, M. Strickland, N. Su, J. High Energy Phys. 1008 (2010) 113.
[35] J.O. Andersen, L.E. Leganger, M. Strickland, N. Su, Phys. Lett. B 696 (2011) 468.
[36] J.O. Andersen, L.E. Leganger, M. Strickland, N. Su, Phys. Rev. D 84 (2011) 087703.
[37] J.O. Andersen, L.E. Leganger, M. Strickland, N. Su, J. High Energy Phys. 1108 (2011) 053.
[38] P. Chakraborty, M.G. Mustafa, M.H. Thoma, Eur. Phys. J. C 23 (2002) 591.
[39] P. Chakraborty, M.G. Mustafa, M.H. Thoma, Phys. Rev. D 68 (2003) 085012.
[40] N. Haque, M.G. Mustafa, M.H. Thoma, Phys. Rev. D 84 (2011) 054009.
[41] N. Haque, M.G. Mustafa, Nuclear Phys. A 862–863 (2011) 271.
[42] N. Haque, M.G. Mustafa, arXiv:1007.2076 [hep-ph].
[43] J.O. Andersen, S. Mogliacci, N. Su, A. Vuorinen, Phys. Rev. D 87 (7) (2013) 074003.
[44] S. Mogliacci, J.O. Andersen, M. Strickland, N. Su, A. Vuorinen, J. High Energy Phys. 1312 (2013) 055.
[45] N. Haque, M.G. Mustafa, M. Strickland, Phys. Rev. D 87 (10) (2013) 105007.
[46] N. Haque, M.G. Mustafa, M. Strickland, J. High Energy Phys. 1307 (2013) 184.
[47] N. Haque, J.O. Andersen, M.G. Mustafa, M. Strickland, N. Su, Phys. Rev. D 89 (6) (2014) 061701.
[48] S. Borsanyi, Z. Fodor, C. Hoelbling, S.D. Katz, S. Krieg, K.K. Szabo, Phys. Lett. B 730 (2014) 99.
[49] Y. Aoki, Z. Fodor, S.D. Katz, K.K. Szabo, J. High Energy Phys. 0601 (2006) 089.
[50] A. Bazavov, et al., HotQCD Collaboration, Phys. Rev. D 90 (2014) 094503.
[51] E. Follana, et al., HPQCD and UKQCD Collaborations, Phys. Rev. D 75 (2007) 054502.
[52] S. Borsanyi, et al., Nature 539 (7627) (2016) 69.
[53] M. Laine, Y. Schroder, Phys. Rev. D 73 (2006) 085009.
[54] M. Asakawa, et al., FlowQCD Collaboration, Phys. Rev. D 90 (1) (2014) 011501, Erratum:; Phys. Rev. D 92 (5) (2015) 059902.
[55] K. Kanaya, S. Ejiri, R. Iwami, M. Kitazawa, H. Suzuki, Y. Taniguchi, T. Umeda, N. Wakabayashi, Proc. Sci. LATTICE2016 (2016) 063.
[56] F. Burger, et al., tmfT Collaboration, Phys. Rev. D 91 (7) (2015) 074504.
[57] S. Pratt, E. Sangaline, P. Sorensen, H. Wang, Phys. Rev. Lett. 114 (2015) 202301.
[58] P. Alba, V. Mantovani Sarti, J. Noronha, J. Noronha-Hostler, P. Parotto, I. Portillo Vazquez, C. Ratti, Phys. Rev. C 98 (3) (2018) 034909.
[59] J.E. Bernhard, J.S. Moreland, S.A. Bass, J. Liu, U. Heinz, Phys. Rev. C 94 (2) (2016) 024907.
[60] J. Auvinen, J.E. Bernhard, S.A. Bass, I. Karpenko, Phys. Rev. C 97 (4) (2018) 044905.
[61] J.O. Andersen, M. Strickland, Phys. Rev. D 66 (2002) 105001, http://dx.doi.org/10.1103/PhysRevD.66.105001, arXiv:hep-ph/0206196 [hep-ph].
[62] E.S. Fraga, A. Kurkela, A. Vuorinen, Astrophys. J. 781 (2014) L25.
[63] E. Annala, T. Gorda, A. Kurkela, J. Nättilä, A. Vuorinen, Nat. Phys. 16 (9) (2020) 907–910, http://dx.doi.org/10.1038/s41567-020-0914-9, arXiv:1903.09121 [astro-ph.HE].
[64] Y. Fujimoto, K. Fukushima, arXiv:2011.10891 [hep-ph].
[65] S. Chandrasekharan, F.J. Jiang, Proc. Sci. LAT2005 (2006) 198, http://dx.doi.org/10.22323/1.020.0198.
[66] P. de Forcrand, M. Fromm, Phys. Rev. Lett. 104 (2010) 112005, http://dx.doi.org/10.1103/PhysRevLett.104.112005, arXiv:0907.1915 [hep-lat].
[67] W. Unger, P. de Forcrand, J. Phys. G 38 (2011) 124190, http://dx.doi.org/10.1088/0954-3899/38/12/124190, arXiv:1107.1553 [hep-lat].
[68] P. de Forcrand, J. Langelage, O. Philipsen, W. Unger, Phys. Rev. Lett. 113 (15) (2014) 152002, http://dx.doi.org/10.1103/PhysRevLett.113.152002, arXiv:1406.4397 [hep-lat].
[69] H. Vairinhos, P. de Forcrand, J. High Energy Phys. 12 (2014) 038, http://dx.doi.org/10.1007/JHEP12(2014)038, arXiv:1409.8442 [hep-lat].
[70] C. Gattringer, Proc. Sci. LATTICE2013 (2014) 002.
[71] C. Marchis, C. Gattringer, Phys. Rev. D 97 (3) (2018) 034508, http://dx.doi.org/10.1103/PhysRevD.97.034508, arXiv:1712.07546 [hep-lat].
[72] R. Leme, O. Oliveira, G. Krein, Eur. Phys. J. C 78 (8) (2018) 656, http://dx.doi.org/10.1140/epjc/s10052-018-6101-9, arXiv:1703.07335 [hep-lat].
[73] P. de Forcrand, W. Unger, H. Vairinhos, Phys. Rev. D 97 (3) (2018) 034512, http://dx.doi.org/10.1103/PhysRevD.97.034512, arXiv:1710.00611 [hep-lat].
[74] F. Bruckmann, J. Wellnhofer, Phys. Rev. D 97 (1) (2018) 014501, http://dx.doi.org/10.1103/PhysRevD.97.014501, arXiv:1710.08243 [hep-lat].
[75] O. Borisenko, V. Chelnokov, S. Voloshyn, EPJ Web Conf. 175 (2018) 11021, http://dx.doi.org/10.1051/epjconf/201817511021, arXiv:1712.03064 [hep-lat].
[76] C. Gattringer, C. Marchis, Nuclear Phys. B 916 (2017) 627–646, http://dx.doi.org/10.1016/j.nuclphysb.2017.01.025, arXiv:1609.00124 [hep-lat].
[77] C. Marchis, C. Gattringer, Proc. Sci. LATTICE2016 (2016) 034, http://dx.doi.org/10.22323/1.256.0034.
[78] C. Gattringer, D. Göschl, C. Marchis, Phys. Lett. B 778 (2018) 435–441, http://dx.doi.org/10.1016/j.physletb.2018.01.065, arXiv:1709.04691 [hep-lat].
[79] M. Cristoforetti, F. Di Renzo, G. Eruzzi, A. Mukherjee, C. Schmidt, L. Scorzato, C. Torrero, Phys. Rev. D 89 (11) (2014) 114505, http://dx.doi.org/10.1103/PhysRevD.89.114505.
[80] A. Alexandru, G. Basar, P.F. Bedaque, G.W. Ridgway, N.C. Warrington, J. High Energy Phys. 1605 (2016) 053.
[81] A. Alexandru, G. Basar, P. Bedaque, Phys. Rev. D 93 (1) (2016) 014504.
[82] L. Scorzato, Proc. Sci. LATTICE2015 (2016) 016.
[83] M. Fukuma, N. Matsumoto, N. Umeda, arXiv:1912.13303 [hep-lat].
[84] F. Di Renzo, S. Singh, K. Zambello, Phys. Rev. D 103 (3) (2021) 034513, http://dx.doi.org/10.1103/PhysRevD.103.034513, arXiv:2008.01622 [hep-lat].
[85] W. Detmold, G. Kanwar, H. Lamm, M.L. Wagman, N.C. Warrington, Phys. Rev. D 103 (9) (2021) 094517, http://dx.doi.org/10.1103/PhysRevD.103.094517, arXiv:2101.12668 [hep-lat].

[86] A. Alexandru, G. Basar, P.F. Bedaque, N.C. Warrington, Rev. Modern Phys. 94 (1) (2022) 015006, http://dx.doi.org/10.1103/RevModPhys.94.015006, arXiv:2007.05436 [hep-lat].
[87] G. Parisi, Y.s. Wu, Sci. Sin. 24 (1981) 483.
[88] P.H. Damgaard, H. Huffel, Phys. Rep. 152 (1987) 227.
[89] G. Aarts, I.O. Stamatescu, J. High Energy Phys. 09 (2008) 018, http://dx.doi.org/10.1088/1126-6708/2008/09/018, arXiv:0807.1597 [hep-lat].
[90] G. Aarts, Phys. Rev. Lett. 102 (2009) 131601, http://dx.doi.org/10.1103/PhysRevLett.102.131601, arXiv:0810.2089 [hep-lat].
[91] G. Aarts, E. Seiler, I.O. Stamatescu, Phys. Rev. D 81 (2010) 054508.
[92] G. Aarts, K. Splittorff, J. High Energy Phys. 08 (2010) 017, http://dx.doi.org/10.1007/JHEP08(2010)017, arXiv:1006.0332 [hep-lat].
[93] G. Aarts, F.A. James, E. Seiler, I.O. Stamatescu, Eur. Phys. J. C 71 (2011) 1756.
[94] G. Aarts, F.A. James, J. High Energy Phys. 01 (2012) 118, http://dx.doi.org/10.1007/JHEP01(2012)118, arXiv:1112.4655 [hep-lat].
[95] G. Aarts, F.A. James, J.M. Pawlowski, E. Seiler, D. Sexty, I.O. Stamatescu, J. High Energy Phys. 03 (2013) 073, http://dx.doi.org/10.1007/JHEP03(2013)073, arXiv:1212.5231 [hep-lat].
[96] E. Seiler, D. Sexty, I.O. Stamatescu, Phys. Lett. B 723 (2013) 213–216, http://dx.doi.org/10.1016/j.physletb.2013.04.062, arXiv:1211.3709 [hep-lat].
[97] D. Sexty, Phys. Lett. B 729 (2014) 108–111, http://dx.doi.org/10.1016/j.physletb.2014.01.019, arXiv:1307.7748 [hep-lat].
[98] A. Mollgaard, K. Splittorff, Phys. Rev. D 88 (11) (2013) 116007.
[99] J. Langelage, M. Neuman, O. Philipsen, J. High Energy Phys. 09 (2014) 131, http://dx.doi.org/10.1007/JHEP09(2014)131, arXiv:1403.4162 [hep-lat].
[100] G. Aarts, E. Seiler, D. Sexty, I.O. Stamatescu, Phys. Rev. D 90 (11) (2014) 114505.
[101] A. Mollgaard, K. Splittorff, Phys. Rev. D 91 (3) (2015) 036007.
[102] K. Splittorff, Phys. Rev. D 91 (3) (2015) 034507.
[103] J. Nishimura, S. Shimasaki, Phys. Rev. D 92 (1) (2015) 011501.
[104] G. Aarts, F. Attanasio, B. Jäger, D. Sexty, J. High Energy Phys. 09 (2016) 087, http://dx.doi.org/10.1007/JHEP09(2016)087.
[105] D.K. Sinclair, J.B. Kogut, Proc. Sci. LATTICE2015 (2016) 153, http://dx.doi.org/10.22323/1.251.0153, arXiv:1510.06367 [hep-lat].
[106] D.K. Sinclair, J.B. Kogut, Proc. Sci. LATTICE2016 (2016) 026, http://dx.doi.org/10.22323/1.256.0026, arXiv:1611.02312 [hep-lat].
[107] C.R. Allton, S. Ejiri, S.J. Hands, O. Kaczmarek, F. Karsch, E. Laermann, C. Schmidt, L. Scorzato, Phys. Rev. D 66 (2002) 074507.
[108] C.R. Allton, M. Doring, S. Ejiri, S.J. Hands, O. Kaczmarek, F. Karsch, E. Laermann, K. Redlich, Phys. Rev. D 71 (2005) 054508.
[109] R.V. Gavai, S. Gupta, Phys. Rev. D 78 (2008) 114503.
[110] S. Basak, et al., MILC, Proc. Sci. LATTICE2008 (2008) 171.
[111] O. Kaczmarek, F. Karsch, E. Laermann, C. Miao, S. Mukherjee, P. Petreczky, C. Schmidt, W. Soeldner, W. Unger, Phys. Rev. D 83 (2011) 014504.
[112] P. de Forcrand, O. Philipsen, Nuclear Phys. B 642 (2002) 290–306.
[113] M. D'Elia, M.P. Lombardo, Phys. Rev. D 67 (2003) 014505.
[114] L.K. Wu, X.Q. Luo, H.S. Chen, Phys. Rev. D 76 (2007) 034505.
[115] M. D'Elia, F. Di Renzo, M.P. Lombardo, Phys. Rev. D 76 (2007) 114509.
[116] S. Conradi, M. D'Elia, Phys. Rev. D 76 (2007) 074501.
[117] P. de Forcrand, O. Philipsen, J. High Energy Phys. 11 (2008) 012.
[118] M. D'Elia, F. Sanfilippo, Phys. Rev. D 80 (2009) 014502.
[119] J.T. Moscicki, M. Wos, M. Lamanna, P. de Forcrand, O. Philipsen, Comput. Phys. Comm. 181 (2010) 1715–1726.
[120] Z. Fodor, S.D. Katz, Phys. Lett. B 534 (2002) 87–92.
[121] Z. Fodor, S.D. Katz, J. High Energy Phys. 03 (2002) 014.
[122] F. Csikor, G.I. Egri, Z. Fodor, S.D. Katz, K.K. Szabo, A.I. Toth, J. High Energy Phys. 05 (2004) 046.
[123] Z. Fodor, S.D. Katz, J. High Energy Phys. 04 (2004) 050.
[124] A. Alexandru, M. Faber, I. Horvath, K.F. Liu, Phys. Rev. D 72 (2005) 114513.
[125] S. Kratochvila, P. de Forcrand, PoS, LAT 2005 (2006) 167.
[126] S. Ejiri, Phys. Rev. D 78 (2008) 074507.
[127] Z. Fodor, S.D. Katz, C. Schmidt, J. High Energy Phys. 03 (2007) 121.
[128] A. Alexandru, C. Gattringer, H.P. Schadler, K. Splittorff, J.J.M. Verbaarschot, Phys. Rev. D 91 (2015) 074501.
[129] K. Langfeld, B. Lucini, A. Rago, Phys. Rev. Lett. 109 (2012) 111601, http://dx.doi.org/10.1103/PhysRevLett.109.111601.
[130] K. Langfeld, J.M. Pawlowski, Phys. Rev. D 88 (7) (2013) 071502, http://dx.doi.org/10.1103/PhysRevD.88.071502.
[131] K. Langfeld, B. Lucini, R. Pellegrini, A. Rago, Eur. Phys. J. C 76 (6) (2016) 306, http://dx.doi.org/10.1140/epjc/s10052-016-4142-5.
[132] N. Garron, K. Langfeld, Eur. Phys. J. C 76 (10) (2016) 569, http://dx.doi.org/10.1140/epjc/s10052-016-4412-2, arXiv:1605.02709 [hep-lat].
[133] K. Langfeld, Proc. Sci. LATTICE2016 (2017) 010, http://dx.doi.org/10.22323/1.256.0010.
[134] N. Garron, K. Langfeld, Eur. Phys. J. C 77 (7) (2017) 470, http://dx.doi.org/10.1140/epjc/s10052-017-5039-7, arXiv:1703.04649 [hep-lat].
[135] M. Giuliani, C. Gattringer, Phys. Lett. B 773 (2017) 166–171, http://dx.doi.org/10.1016/j.physletb.2017.08.014, arXiv:1703.03614 [hep-lat].
[136] S. Borsanyi, D. Sexty, Phys. Lett. B 815 (2021) 136148, http://dx.doi.org/10.1016/j.physletb.2021.136148.
[137] R. Bellwied, S. Borsanyi, Z. Fodor, J. Günther, S. Katz, C. Ratti, K. Szabo, Phys. Lett. B 751 (2015) 559–564.
[138] J.N. Guenther, R. Bellwied, S. Borsanyi, Z. Fodor, S.D. Katz, A. Pasztor, C. Ratti, K.K. Szabó, Nuclear Phys. A 967 (2017) 720–723.
[139] S. Borsanyi, Z. Fodor, J.N. Guenther, S.K. Katz, K.K. Szabo, A. Pasztor, I. Portillo, C. Ratti, J. High Energy Phys. 10 (2018) 205.
[140] S. Borsanyi, G. Endrodi, Z. Fodor, S.D. Katz, S. Krieg, C. Ratti, K.K. Szabo, J. High Energy Phys. 08 (2012) 053.
[141] P. Hegde, BNL/Bielefeld/CCNU, Nuclear Phys. A 931 (2014) 851–855.
[142] P. Alba, W. Alberico, R. Bellwied, M. Bluhm, V. Mantovani Sarti, M. Nahrgang, C. Ratti, Phys. Lett. B 738 (2014) 305–310.
[143] T. Dore, J. Karthein, D. Mroczek, P. Parotto, J. Noronha-Hostler, C. Ratti, arXiv:2109.05098 [nucl-th].
[144] A. Bazavov, H. Ding, P. Hegde, O. Kaczmarek, F. Karsch, E. Laermann, Y. Maezawa, S. Mukherjee, H. Ohno, P. Petreczky, H. Sandmeyer, P. Steinbrecher, C. Schmidt, S. Sharma, W. Soeldner, M. Wagner, Phys. Rev. D 95 (5) (2017) 054504.
[145] M. D'Elia, G. Gagliardi, F. Sanfilippo, Phys. Rev. D 95 (9) (2017) 094503.
[146] J. Noronha-Hostler, P. Parotto, C. Ratti, J.M. Stafford, Phys. Rev. C 100 (6) (2019) 064910.
[147] A. Monnai, B. Schenke, C. Shen, Phys. Rev. C 100 (2) (2019) 024907.
[148] S. Mondal, S. Mukherjee, P. Hegde, arXiv:2106.03165 [hep-lat].
[149] R. Bellwied, S. Borsanyi, Z. Fodor, J.N. Guenther, J. Noronha-Hostler, P. Parotto, A. Pasztor, C. Ratti, J.M. Stafford, Phys. Rev. D 101 (3) (2020) 034506, http://dx.doi.org/10.1103/PhysRevD.101.034506, arXiv:1910.14592 [hep-lat].
[150] R. Bellwied, S. Borsanyi, Z. Fodor, S.D. Katz, A. Pasztor, C. Ratti, K.K. Szabo, Phys. Rev. D 92 (11) (2015) 114505, http://dx.doi.org/10.1103/PhysRevD.92.114505, arXiv:1507.04627 [hep-lat].
[151] S. Borsanyi, Z. Fodor, J.N. Guenther, R. Kara, P. Parotto, A. Pasztor, C. Ratti, K.K. Szabo, arXiv:2202.05574 [hep-lat].
[152] S. Borsanyi, et al., Wuppertal-Budapest, J. High Energy Phys. 09 (2010) 073.
[153] G. Aarts, J. Phys. Conf. Ser. 706 (2) (2016) 022004.
[154] G. Endrodi, Z. Fodor, S.D. Katz, K.K. Szabo, J. High Energy Phys. 04 (2011) 001.

[155] P. Cea, L. Cosmai, A. Papa, Phys. Rev. D 93 (1) (2016) 014507.
[156] C. Bonati, M. D'Elia, M. Mariti, M. Mesiti, F. Negro, F. Sanfilippo, Phys. Rev. D 92 (5) (2015) 054503.
[157] S. Borsanyi, Z. Fodor, J.N. Guenther, R. Kara, S.D. Katz, P. Parotto, A. Pasztor, C. Ratti, K.K. Szabo, Phys. Rev. Lett. 125 (5) (2020) 052001.
[158] C. Bonati, M. D'Elia, F. Negro, F. Sanfilippo, K. Zambello, Phys. Rev. D 98 (5) (2018) 054510.
[159] A. Bazavov, et al., HotQCD, Phys. Lett. B 795 (2019) 15–21.
[160] P. Cea, L. Cosmai, A. Papa, Phys. Rev. D 89 (7) (2014) 074512.
[161] C. Bonati, M. D'Elia, M. Mariti, M. Mesiti, F. Negro, F. Sanfilippo, Phys. Rev. D 90 (11) (2014) 114025.
[162] P. Hegde, et al., Bielefeld-BNL-CCNU, Proc. Sci. LATTICE2015 (2016) 141.
[163] A.M. Halasz, A. Jackson, R. Shrock, M.A. Stephanov, J. Verbaarschot, Phys. Rev. D 58 (1998) 096007.
[164] M.A. Stephanov, Progr. Theoret. Phys. Suppl. 153 (2004) 139–156.
[165] A. Bzdak, S. Esumi, V. Koch, J. Liao, M. Stephanov, N. Xu, Phys. Rep. 853 (2020) 1–87.
[166] R. Gavai, S. Gupta, Phys. Rev. D 71 (2005) 114014.
[167] F. Karsch, B. Schaefer, M. Wagner, J. Wambach, Proc. Sci. LATTICE2011 (2011) 219.
[168] Z. Fodor, M. Giordano, J.N. Günther, K. Kapás, S.D. Katz, A. Pásztor, I. Portillo, C. Ratti, D. Sexty, K.K. Szabó, Nuclear Phys. A 982 (2019) 843–846.
[169] P. Steinbrecher, HotQCD, Proc. Sci. LATTICE2018 (2018) 160.
[170] S. Datta, R.V. Gavai, S. Gupta, Phys. Rev. D 95 (5) (2017) 054512.
[171] S. Borsanyi, Z. Fodor, J.N. Guenther, R. Kara, S.D. Katz, P. Parotto, A. Pasztor, C. Ratti, K.K. Szabo, Phys. Rev. Lett. 125 (5) (2020) 052001, http://dx.doi.org/10.1103/PhysRevLett.125.052001, arXiv:2002.02821 [hep-lat].
[172] S. Borsanyi, Z. Fodor, S.D. Katz, S. Krieg, C. Ratti, K. Szabo, J. High Energy Phys. 01 (2012) 138.
[173] A. Bazavov, et al., HotQCD, Phys. Rev. D 86 (2012) 034509.
[174] R. Bellwied, S. Borsanyi, Z. Fodor, S.D. Katz, A. Pasztor, C. Ratti, K.K. Szabo, Phys. Rev. D 92 (11) (2015) 114505.
[175] H.T. Ding, S. Mukherjee, H. Ohno, P. Petreczky, H.P. Schadler, Phys. Rev. D 92 (7) (2015) 074043.
[176] N. Haque, A. Bandyopadhyay, J.O. Andersen, M.G. Mustafa, M. Strickland, N. Su, J. High Energy Phys. 05 (2014) 027.
[177] S. Mogliacci, J.O. Andersen, M. Strickland, N. Su, A. Vuorinen, J. High Energy Phys. 12 (2013) 055.
[178] R. Bellwied, S. Borsanyi, Z. Fodor, S.D. Katz, C. Ratti, Phys. Rev. Lett. 111 (2013) 202302.
[179] S. Borsanyi, Z. Fodor, S.D. Katz, S. Krieg, C. Ratti, K.K. Szabo, Phys. Rev. Lett. 111 (2013) 062005.
[180] A. Bazavov, D. Bollweg, H.T. Ding, P. Enns, J. Goswami, P. Hegde, O. Kaczmarek, F. Karsch, R. Larsen, S. Mukherjee, H. Ohno, P. Petreczky, C. Schmidt, S. Sharma, P. Steinbrecher, Phys. Rev. D 101 (7) (2020) 074502.
[181] M. D'Elia, G. Gagliardi, F. Sanfilippo, Phys. Rev. D 95 (9) (2017) 094503.
[182] A. Bazavov, H.T. Ding, P. Hegde, O. Kaczmarek, F. Karsch, E. Laermann, S. Mukherjee, P. Petreczky, C. Schmidt, D. Smith, W. Soeldner, M. Wagner, Phys. Rev. Lett. 109 (2012) 192302.
[183] N.R. Sahoo, STAR, Acta Phys. Polon. Suppl. 6 (2013) 437–444.
[184] S. Borsanyi, Z. Fodor, S.D. Katz, S. Krieg, C. Ratti, K.K. Szabo, Phys. Rev. Lett. 113 (2014) 052301.
[185] J. Noronha-Hostler, R. Bellwied, J. Gunther, P. Parotto, A. Pasztor, I. Portillo Vazquez, C. Ratti, arXiv:1607.02527 [hep-ph].
[186] P. Alba, W. Alberico, R. Bellwied, M. Bluhm, V. Mantovani Sarti, M. Nahrgang, C. Ratti, Phys. Lett. B 738 (2014) 305–310, http://dx.doi.org/10.1016/j.physletb.2014.09.052, arXiv:1403.4903 [hep-ph].
[187] A. Bazavov, H.T. Ding, P. Hegde, O. Kaczmarek, F. Karsch, E. Laermann, Y. Maezawa, S. Mukherjee, H. Ohno, P. Petreczky, C. Schmidt, S. Sharma, W. Soeldner, M. Wagner, Phys. Rev. Lett. 111 (2013) 082301.
[188] P. Alba, R. Bellwied, S. Borsanyi, Z. Fodor, J. Günther, S.D. Katz, V. Mantovani Sarti, J. Noronha-Hostler, P. Parotto, A. Pasztor, I. Portillo Vazquez, C. Ratti, Phys. Rev. D 96 (3) (2017) 034517.
[189] F. Karsch, K. Redlich, A. Tawfik, Eur. Phys. J. C 29 (2003) 549–556.
[190] F. Karsch, K. Redlich, A. Tawfik, Phys. Lett. B 571 (2003) 67–74.
[191] K. Redlich, F. Karsch, A. Tawfik, J. Phys. G 30 (2004) S1271–S1274.
[192] C. Ratti, M.A. Thaler, W. Weise, arXiv:nucl-th/0604025 [nucl-th].
[193] P. Huovinen, P. Petreczky, Nuclear Phys. A 837 (2010) 26–53.
[194] P. Huovinen, P. Petreczky, J. Phys. Conf. Ser. 230 (2010) 012012.
[195] C. Ratti, et al., [Wuppertal-Budapest], Nuclear Phys. A 855 (2011) 253–256, http://dx.doi.org/10.1016/j.nuclphysa.2011.02.052, arXiv:1012.5215 [hep-lat].
[196] M. Ruggieri, P. Alba, P. Castorina, S. Plumari, C. Ratti, V. Greco, Phys. Rev. D 86 (2012) 054007, http://dx.doi.org/10.1103/PhysRevD.86.054007, arXiv:1204.5995 [hep-ph].
[197] A. Bazavov, H.T. Ding, P. Hegde, O. Kaczmarek, F. Karsch, E. Laermann, Y. Maezawa, S. Mukherjee, H. Ohno, P. Petreczky, C. Schmidt, S. Sharma, W. Soeldner, M. Wagner, Phys. Rev. Lett. 113 (7) (2014) 072001.
[198] P. Alba, V. Mantovani Sarti, J. Noronha, J. Noronha-Hostler, P. Parotto, I. Portillo Vazquez, C. Ratti, Phys. Rev. C 98 (3) (2018) 034909.
[199] P. Alba, V.M. Sarti, J. Noronha-Hostler, P. Parotto, I. Portillo-Vazquez, C. Ratti, J.M. Stafford, Phys. Rev. C 101 (5) (2020) 054905.
[200] V. Vovchenko, M.I. Gorenstein, H. Stoecker, Phys. Rev. Lett. 118 (18) (2017) 182301.
[201] P.M. Lo, B. Friman, K. Redlich, C. Sasaki, Phys. Lett. B 778 (2018) 454–458.
[202] J.M. Karthein, V. Koch, C. Ratti, V. Vovchenko, arXiv:2107.00588 [nucl-th].
[203] D. Bollweg, J. Goswami, O. Kaczmarek, F. Karsch, S. Mukherjee, P. Petreczky, C. Schmidt, P. Scior, arXiv:2107.10011 [hep-lat].
[204] C.S. Fischer, Prog. Part. Nucl. Phys. 105 (2019) 1–60, http://dx.doi.org/10.1016/j.ppnp.2019.01.002, arXiv:1810.12938 [hep-ph].
[205] F. Gao, J. Chen, Y.X. Liu, S.X. Qin, C.D. Roberts, S.M. Schmidt, Phys. Rev. D 93 (9) (2016) 094019, http://dx.doi.org/10.1103/PhysRevD.93.094019, arXiv:1507.00875 [nucl-th].
[206] F. Gao, Y. x. Liu, Phys. Rev. D 94 (9) (2016) 094030, http://dx.doi.org/10.1103/PhysRevD.94.094030, arXiv:1609.08038 [hep-ph].
[207] X.y. Xin, S.x. Qin, Y.x. Liu, Phys. Rev. D 90 (7) (2014) 076006, http://dx.doi.org/10.1103/PhysRevD.90.076006, arXiv:2109.09935 [hep-ph].
[208] P. Isserstedt, C.S. Fischer, T. Steinert, Phys. Rev. D 103 (5) (2021) 054012, http://dx.doi.org/10.1103/PhysRevD.103.054012, arXiv:2012.04991 [hep-ph].
[209] T.K. Herbst, M. Mitter, J.M. Pawlowski, B.J. Schaefer, R. Stiele, Phys. Lett. B 731 (2014) 248–256, http://dx.doi.org/10.1016/j.physletb.2014.02.045, arXiv:1308.3621 [hep-ph].
[210] F. Rennecke, B.J. Schaefer, Phys. Rev. D 96 (1) (2017) 016009, http://dx.doi.org/10.1103/PhysRevD.96.016009, arXiv:1610.08748 [hep-ph].
[211] W.j. Fu, J.M. Pawlowski, F. Rennecke, SciPost Phys. Core 2 (2020) 002, http://dx.doi.org/10.21468/SciPostPhysCore.2.1.002, arXiv:1808.00410 [hep-ph].
[212] W.j. Fu, J.M. Pawlowski, F. Rennecke, Phys. Rev. D 100 (11) (2019) 111501, http://dx.doi.org/10.1103/PhysRevD.100.111501, arXiv:1809.01594 [hep-ph].
[213] J.M. Pawlowski, Nuclear Phys. A 931 (2014) 113–124, http://dx.doi.org/10.1016/j.nuclphysa.2014.09.074.
[214] W.j. Fu, X. Luo, J.M. Pawlowski, F. Rennecke, R. Wen, S. Yin, Phys. Rev. D 104 (9) (2021) 9, http://dx.doi.org/10.1103/PhysRevD.104.094047, arXiv:2101.06035 [hep-ph].

[215] O. DeWolfe, S.S. Gubser, C. Rosen, Phys. Rev. D 83 (2011) 086005.
[216] R. Rougemont, R. Critelli, J. Noronha-Hostler, J. Noronha, C. Ratti, Phys. Rev. D 96 (1) (2017) 014032.
[217] J.M. Maldacena, Internat. J. Theoret. Phys. 38 (1999) 1113–1133.
[218] R. Critelli, J. Noronha, J. Noronha-Hostler, I. Portillo, C. Ratti, R. Rougemont, Phys. Rev. D 96 (9) (2017) 096026.
[219] S.S. Gubser, A. Nellore, S.S. Pufu, F.D. Rocha, Phys. Rev. Lett. 101 (2008) 131601, http://dx.doi.org/10.1103/PhysRevLett.101.131601, arXiv:0804.1950 [hep-th].
[220] O. DeWolfe, S.S. Gubser, C. Rosen, Phys. Rev. D 84 (2011) 126014, http://dx.doi.org/10.1103/PhysRevD.84.126014, arXiv:1108.2029 [hep-th].
[221] P. Kovtun, D.T. Son, A.O. Starinets, Phys. Rev. Lett. 94 (2005) 111601, http://dx.doi.org/10.1103/PhysRevLett.94.111601, arXiv:hep-th/0405231 [hep-th].
[222] J. Casalderrey-Solana, H. Liu, D. Mateos, K. Rajagopal, U.A. Wiedemann, http://dx.doi.org/10.1017/CBO9781139136747. arXiv:1101.0618 [hep-th].
[223] A. Ficnar, J. Noronha, M. Gyulassy, Nuclear Phys. A 855 (2011) 372–375, http://dx.doi.org/10.1016/j.nuclphysa.2011.02.083, arXiv:1012.0116 [hep-ph].
[224] A. Ficnar, J. Noronha, M. Gyulassy, J. Phys. G 38 (2011) 124176, http://dx.doi.org/10.1088/0954-3899/38/12/124176, arXiv:1106.6303 [hep-ph].
[225] A. Ficnar, J. Noronha, M. Gyulassy, Nuclear Phys. A 910–911 (2013) 252–255, http://dx.doi.org/10.1016/j.nuclphysa.2012.12.030, arXiv:1208.0305 [hep-ph].
[226] S.I. Finazzo, J. Noronha, Phys. Rev. D 89 (10) (2014) 106008, http://dx.doi.org/10.1103/PhysRevD.89.106008, arXiv:1311.6675 [hep-th].
[227] S.I. Finazzo, R. Rougemont, H. Marrochio, J. Noronha, J. High Energy Phys. 02 (2015) 051, http://dx.doi.org/10.1007/JHEP02(2015)051, arXiv:1412.2968 [hep-ph].
[228] R. Rougemont, J. Noronha, J. Noronha-Hostler, Phys. Rev. Lett. 115 (20) (2015) 202301, http://dx.doi.org/10.1103/PhysRevLett.115.202301.
[229] R. Rougemont, A. Ficnar, S. Finazzo, J. Noronha, J. High Energy Phys. 04 (2016) 102, http://dx.doi.org/10.1007/JHEP04(2016)102, arXiv:1507.06556 [hep-th].
[230] S.I. Finazzo, R. Rougemont, Phys. Rev. D 93 (3) (2016) 034017, http://dx.doi.org/10.1103/PhysRevD.93.034017.
[231] R. Rougemont, R. Critelli, J. Noronha-Hostler, J. Noronha, C. Ratti, Phys. Rev. D 96 (1) (2017) 014032, http://dx.doi.org/10.1103/PhysRevD.96.014032, arXiv:1704.05558 [hep-ph].
[232] R. Rougemont, R. Critelli, J. Noronha, Phys. Rev. D 98 (3) (2018) 034028, http://dx.doi.org/10.1103/PhysRevD.98.034028, arXiv:1804.00189 [hep-ph].
[233] R. Rougemont, R. Critelli, J. Noronha, Phys. Rev. D 93 (4) (2016) 045013, http://dx.doi.org/10.1103/PhysRevD.93.045013, arXiv:1505.07894 [hep-th].
[234] S.I. Finazzo, R. Critelli, R. Rougemont, J. Noronha, Phys. Rev. D 94 (5) (2016) 054020, http://dx.doi.org/10.1103/PhysRevD.94.054020, arXiv:1605.06061 [hep-ph]. erratum:; Phys. Rev. D 96 (1) (2017) 019903.
[235] R. Critelli, R. Rougemont, S.I. Finazzo, J. Noronha, Phys. Rev. D 94 (12) (2016) 125019, http://dx.doi.org/10.1103/PhysRevD.94.125019, arXiv:1606.09484 [hep-ph].
[236] R. Rougemont, Phys. Rev. D 102 (3) (2020) 034009, http://dx.doi.org/10.1103/PhysRevD.102.034009, arXiv:2002.06725 [hep-ph].
[237] R. Yaresko, J. Knaute, B. Kämpfer, Eur. Phys. J. C 75 (6) (2015) 295, http://dx.doi.org/10.1140/epjc/s10052-015-3513-7, arXiv:1503.09065 [hep-ph].
[238] J. Knaute, B. Kämpfer, Phys. Rev. D 96 (10) (2017) 106003, http://dx.doi.org/10.1103/PhysRevD.96.106003, arXiv:1706.02647 [hep-ph].
[239] J. Knaute, R. Yaresko, B. Kämpfer, Phys. Lett. B 778 (2018) 419–425, http://dx.doi.org/10.1016/j.physletb.2018.01.053, arXiv:1702.06731 [hep-ph].
[240] Z. Li, Y. Chen, D. Li, M. Huang, Chin. Phys. C 42 (1) (2018) 013103, http://dx.doi.org/10.1088/1674-1137/42/1/013103, arXiv:1706.02238 [hep-ph].
[241] R.G. Cai, S. He, L. Li, Y.X. Wang, arXiv:2201.02004 [hep-th].
[242] J. Grefa, M. Hippert, J. Noronha, J. Noronha-Hostler, I. Portillo, C. Ratti, R. Rougemont, arXiv:2203.00139 [nucl-th].
[243] M. Attems, J. Casalderrey-Solana, D. Mateos, I. Papadimitriou, D. Santos-Oliván, C.F. Sopuerta, M. Triana, M. Zilhão, J. High Energy Phys. 10 (2016) 155, http://dx.doi.org/10.1007/JHEP10(2016)155, arXiv:1603.01254 [hep-th].
[244] M. Attems, Y. Bea, J. Casalderrey-Solana, D. Mateos, M. Triana, M. Zilhão, Phys. Rev. Lett. 121 (26) (2018) 261601, http://dx.doi.org/10.1103/PhysRevLett.121.261601, arXiv:1807.05175 [hep-th].
[245] M. Attems, J. High Energy Phys. 08 (2021) 155, http://dx.doi.org/10.1007/JHEP08(2021)155, arXiv:2012.15687 [hep-th].
[246] J. Grefa, J. Noronha, J. Noronha-Hostler, I. Portillo, C. Ratti, R. Rougemont, Phys. Rev. D 104 (3) (2021) 034002, http://dx.doi.org/10.1103/PhysRevD.104.034002, arXiv:2102.12042 [nucl-th].
[247] K. Rajagopal, F. Wilczek, Nuclear Phys. B 399 (1993) 395–425.
[248] J. Berges, K. Rajagopal, Nuclear Phys. B 538 (1999) 215–232.
[249] F. Karsch, E. Laermann, C. Schmidt, Phys. Lett. B 520 (2001) 41–49.
[250] P. de Forcrand, O. Philipsen, Nuclear Phys. B 673 (2003) 170–186.
[251] P. Parotto, M. Bluhm, D. Mroczek, M. Nahrgang, J. Noronha-Hostler, K. Rajagopal, C. Ratti, T. Schäfer, M. Stephanov, Phys. Rev. C 101 (3) (2020) 034901.
[252] J.M. Karthein, D. Mroczek, A.R. Nava Acuna, J. Noronha-Hostler, P. Parotto, D.R.P. Price, C. Ratti, Eur. Phys. J. Plus 136 (6) (2021) 621, http://dx.doi.org/10.1140/epjp/s13360-021-01615-5, arXiv:2103.08146 [hep-ph].
[253] B.B. Brandt, G. Endrodi, S. Schmalzbauer, Phys. Rev. D 97 (5) (2018) 054514.
[254] C. Ratti, W. Weise, Phys. Rev. D 70 (2004) 054013.
[255] J.O. Andersen, T. Brauner, Phys. Rev. D 81 (2010) 096004.
[256] T. Zhang, T. Brauner, D.H. Rischke, J. High Energy Phys. 06 (2010) 064.
[257] N. Strodthoff, B.J. Schaefer, L. von Smekal, Phys. Rev. D 85 (2012) 074007.
[258] T. Xia, L. He, P. Zhuang, Phys. Rev. D 88 (5) (2013) 056013.
[259] B.B. Brandt, F. Cuteri, G. Endrodi, arXiv:2110.14750 [hep-lat].
[260] B.B. Brandt, G. Endrodi, E.S. Fraga, M. Hippert, J. Schaffner-Bielich, S. Schmalzbauer, Phys. Rev. D 98 (9) (2018) 094510, http://dx.doi.org/10.1103/PhysRevD.98.094510, arXiv:1802.06685 [hep-ph].
[261] S. Borsanyi, Z. Fodor, M. Giordano, S.D. Katz, D. Nogradi, A. Pasztor, C.H. Wong, Phys. Rev. D 105 (5) (2022) L051506, http://dx.doi.org/10.1103/PhysRevD.105.L051506, arXiv:2108.09213 [hep-lat].
[262] J. Engels, F. Karsch, H. Satz, I. Montvay, Nuclear Phys. B 205 (1982) 545–577.
[263] Y. Deng, Nucl. Phys. B (Proc. Suppl.) 9 (1989) 334.
[264] R.V. Gavai, S. Gupta, S. Mukherjee, Pramana 71 (2008) 487–508.
[265] S. Mukherjee, QCD Thermodynamics from Lattice Gauge Theory (Ph. D. Thesis), 2006.
[266] A. Hasenfratz, P. Hasenfratz, Nuclear Phys. B 193 (1981) 210.
[267] J. Engels, J. Fingberg, F. Karsch, D. Miller, M. Weber, Phys. Lett. B 252 (1990) 625–630.
[268] G. Boyd, J. Engels, F. Karsch, E. Laermann, C. Legeland, M. Lutgemeier, B. Petersson, Phys. Rev. Lett. 75 (1995) 4169–4172.
[269] G. Boyd, J. Engels, F. Karsch, E. Laermann, C. Legeland, M. Lutgemeier, B. Petersson, Nuclear Phys. B 469 (1996) 419–444.